JOURNAL OF PETROLOGY | VOLUME 47 | NUMBER 3 | PAGES 541–566 | 2006 | doi:10.1093/petrology/egi085

Overlap of Karoo and Ferrar Magma Types in KwaZulu-Natal, South Africa

T. R. RILEY[1]*, M. L. CURTIS[1], P. T. LEAT[1], M. K. WATKEYS[2], R. A. DUNCAN[3], I. L. MILLAR[4] AND W. H. OWENS[5]

[1]BRITISH ANTARCTIC SURVEY, HIGH CROSS, MADINGLEY ROAD, CAMBRIDGE, CB3 0ET, UK

[2]SCHOOL OF GEOLOGICAL AND COMPUTER SCIENCES, UNIVERSITY OF KWAZULU-NATAL, DURBAN 4041, SOUTH AFRICA

[3]COLLEGE OF OCEANIC AND ATMOSPHERIC SCIENCES, OREGON STATE UNIVERSITY, CORVALLIS, OR 97331-5503, USA

[4]BRITISH ANTARCTIC SURVEY, c/o NERC ISOTOPE GEOSCIENCES LABORATORY, KEYWORTH, NOTTINGHAM NG12 5GG, UK

[5]SCHOOL OF GEOGRAPHY, EARTH AND ENVIRONMENTAL SCIENCES, UNIVERSITY OF BIRMINGHAM, BIRMINGHAM B15 2TT, UK

RECEIVED JULY 16, 2004; ACCEPTED OCTOBER 18, 2005
ADVANCE ACCESS PUBLICATION DECEMBER 8, 2005

A suite of mafic dykes from the Underberg region of southern KwaZulu-Natal (South Africa) were intruded at ~178 Ma, coincident in age with the major Okavango Dyke Swarm of Botswana, and also coincident with minor Karoo-related intrusions of the northern and central Lebombo. The dykes are all low-Ti–Zr tholeiites, they trend NW–SE and are presumed to continue into the Karoo central area of the Lesotho Highlands. In many respects, the Underberg dykes are similar to the majority of the low-Ti–Zr volcanic and subvolcanic intrusions of the Karoo; however, their $^{87}Sr/^{86}Sr$ and εNd isotope ratios are either 'Ferrar-like' ($^{87}Sr/^{86}Sr \sim 0{\cdot}710$; $\varepsilon Nd < -3$) or transitional between Karoo low-Ti–Zr and Ferrar low-Ti magmas. A potential Ferrar source for at least some of the Underberg dykes is supported by anisotropy of magnetic susceptibility analyses of the dyke suite, which demonstrate absolute flow direction from the SE to the NW, consistent with Gondwana reconstructions. The role of crustal contamination and combined fractional crystallization is also demonstrated to have played a key role in the petrogenesis of the Underberg dykes, involving a local upper crust contaminant. However, the composition of the 'Ferrar-like' dykes cannot be easily explained by AFC processes, but they do demonstrate that melting of a lithospheric mantle source enriched to a small degree by subduction-derived fluid was also important.

KEY WORDS: *dyke; basalt; crustal contamination; large igneous province*

INTRODUCTION

Remnants of the Early Jurassic Karoo and Ferrar large igneous provinces (LIPs) are distributed across large parts of southern Africa and East Antarctica (Fig. 1). The geochemistry of the Karoo igneous rocks has been interpreted by a number of workers to indicate either derivation from an enriched lithospheric mantle source (e.g. Erlank, 1984) or crustal contamination of magmas derived from a lithospheric source. Others have proposed that the Karoo magmas were partial melts of a mantle plume source that were subsequently contaminated by lithospheric mantle components (Cox, 1992; Ellam *et al.*, 1992; Sweeney *et al.*, 1994).

The Ferrar province (Fig. 1), although essentially contemporaneous (Riley & Knight, 2001) with the Karoo volcanic province, is considerably different in chemistry. The erupted rocks of the Ferrar province are characterized by high SiO_2, low TiO_2, radiogenic $^{87}Sr/^{86}Sr$ (Kyle, 1980) and negative εNd, which has led several workers (e.g. Antonini *et al.*, 1999) to suggest that processes involving contamination of the magmas by continental crust must have been important (e.g. Faure *et al.*, 1974). Other workers (e.g. Kyle, 1980; Hergt, 2000) maintain that continental crust was not involved in the petrogenesis of Ferrar magmas, supported by their 'mantle-like' Os isotope ratios (Molzahn *et al.*, 1996), and that their

*Corresponding author. E-mail: t-riley@bas.ac.uk

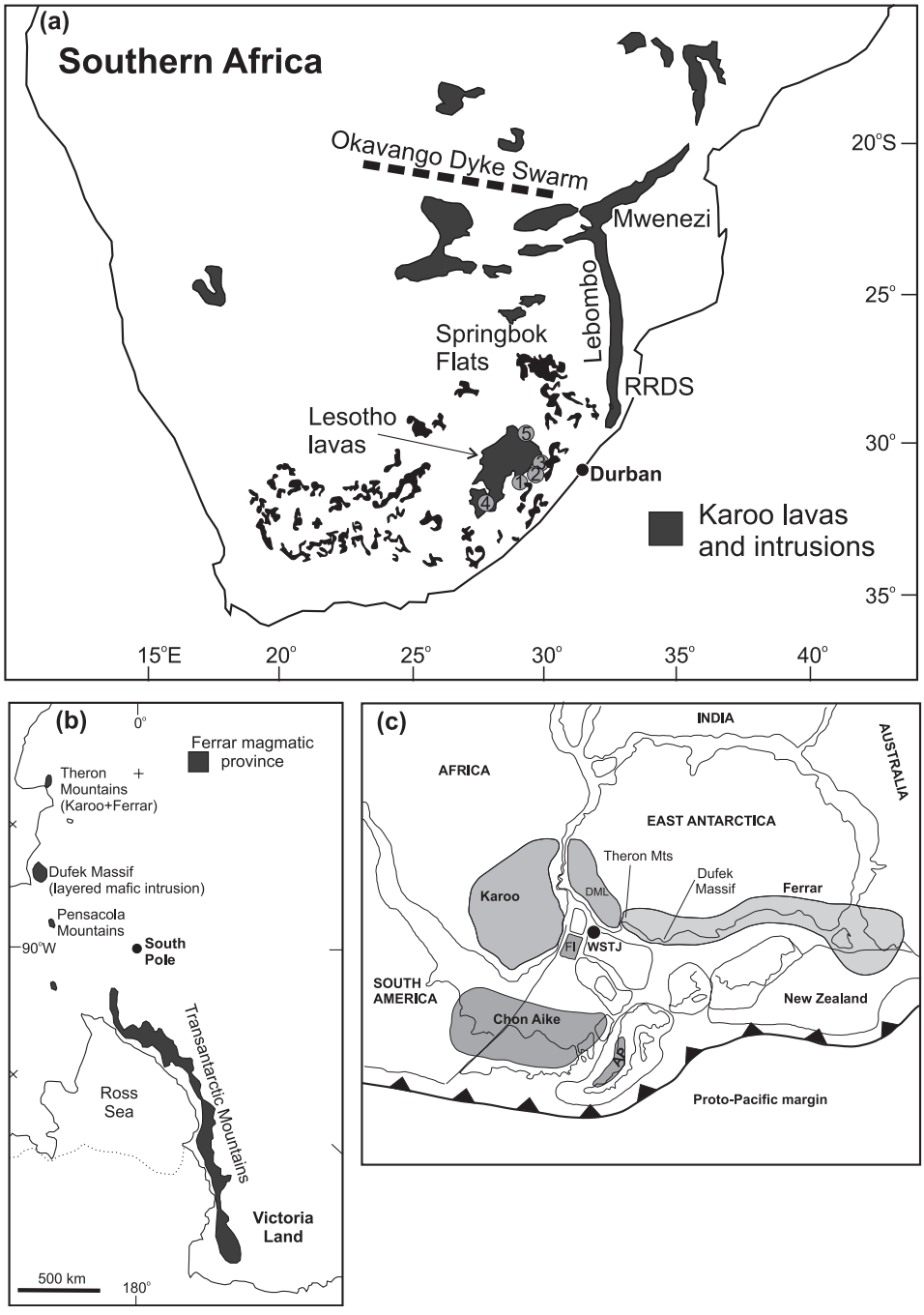

Fig. 1. (a) Geological extent of the Karoo province in southern Africa. The major lava units and sill complexes are highlighted, along with the Okavango dyke swarm and the Rooi Rand dyke swarm (RRDS). 1, New Amalfi Sheet; 2, Underberg; 3, Sani Pass; 4, Moshesh's Ford; 5, Monotsha Pass and Golden Gate. (b) Geological extent of the Ferrar magmatic province in East Antarctica. The Theron Mountains may be an area where Karoo and Ferrar magma types overlap. (c) Pre-break-up Gondwana reconstruction (~180 Ma) showing key igneous provinces of the Karoo, Ferrar, and Chon Aike. FI, Falkland Islands; DML, Dronning Maud Land; WSTJ, Weddell Sea triple junction (Elliot & Fleming, 2000); AP, Antarctic Peninsula.

radiogenic $^{87}Sr/^{86}Sr$ is a characteristic of their mantle source. Central to the debate concerning the origin of any flood basalt province is establishing whether a mantle plume source existed and determining whether the role of the plume was restricted to conductive heat transfer to the lithosphere, or whether uncontaminated plume-derived magmas were erupted at the surface or intruded at upper crustal levels.

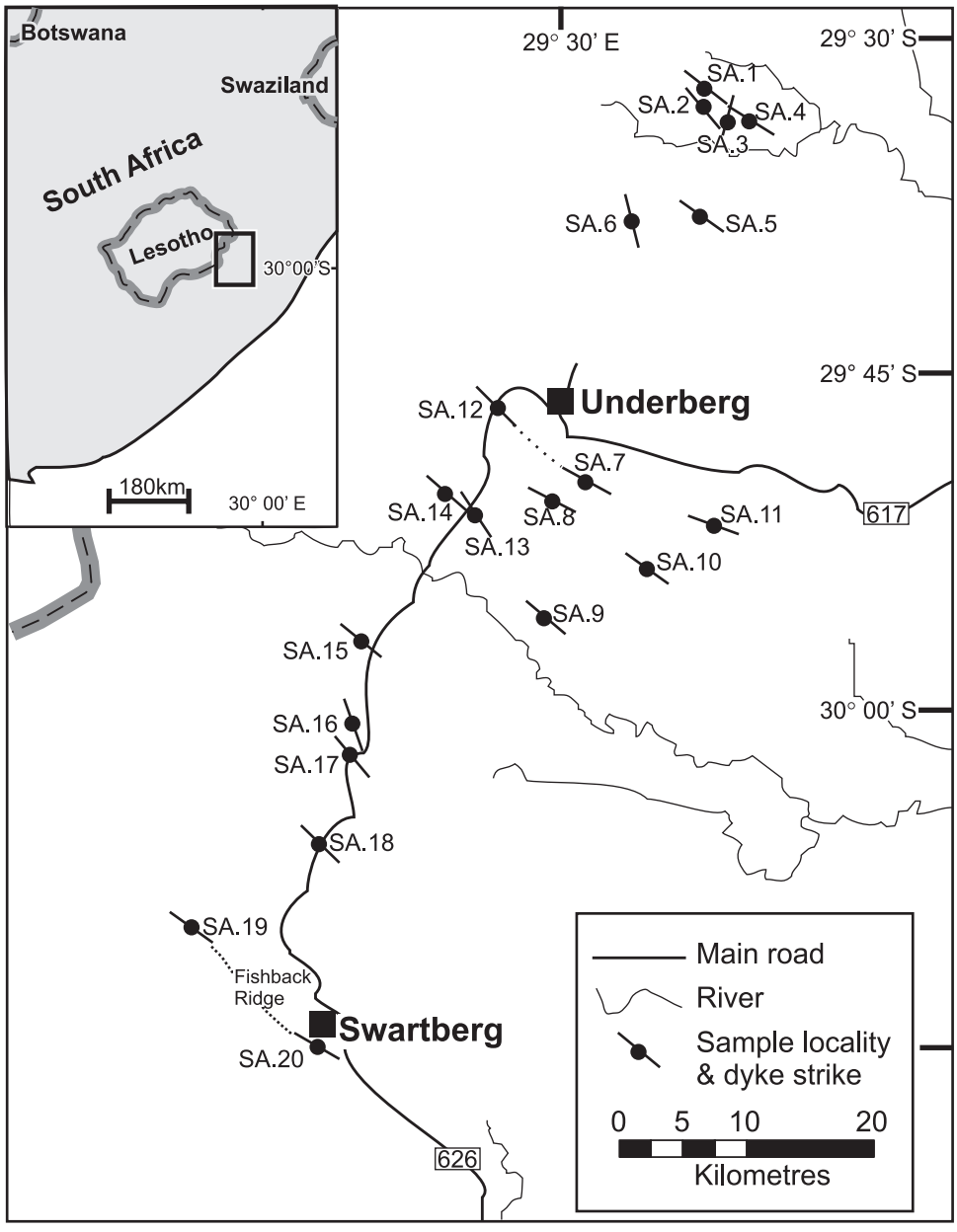

Fig. 2. Distribution of dyke localities in the Underberg region of southern KwaZulu-Natal (South Africa). Lines on the sample locality indicate the strike direction of the dyke. Dashed lines indicate the probable continuation of dykes.

A suite of mafic dykes from the Underberg region of southern KwaZulu-Natal Province of South Africa (Fig. 2) crop out in an area where, based on previous geochemical studies (Elliot *et al.*, 1999), Karoo and Ferrar magmatic provinces may overlap. We present the results of geochemical, geochronological and magma flow studies to constrain the petrogenesis of the dykes and to improve understanding of the relationship between the Karoo and Ferrar flood basalt provinces.

GEOLOGICAL SETTING

The intracratonic Karoo sedimentary sequence was deposited, from Permo-Carboniferous to Early Jurassic times, in a basin overlying the Archaean Kaapvaal Craton in the north and on the Proterozoic Namaqua–Natal Belt and Paleozoic Cape Supergroup in the south (Smith, 1990). The main sedimentary formations, with a total thickness $\leq$6 km, are named, from base to top: Dwyka, Ecca, Beaufort, Molteno, Elliot

and Clarens. The Karoo igneous event, with the emplacement of the volcanic Drakensberg Group, marked the end of the Karoo basin evolution. This event consisted in the continental-scale eruption of tholeiitic basalt lavas and the intrusion of numerous dykes and sills of similar composition at 183 ± 1 Ma. Present-day outcrops of Karoo volcanic rocks are concentrated in the central area of the Karoo (predominantly Lesotho), the Lebombo rifted margin and NE Botswana, with local concentrations occurring elsewhere in South Africa, Botswana, Namibia and western Dronning Maud Land (Antarctica) (Fig. 1). Intrusive rocks of the Karoo volcanic province are more widespread, with a vast sill complex (Fig. 1) distributed over much of South Africa and Namibia (Chevallier & Woodford, 1999), and major dyke swarms occurring in Botswana (Okavango and south Botswana) and southern Lebombo (Rooi Rand).

The Karoo volcanic province has been divided into high- and low-Ti–Zr basalts (Cox *et al.*, 1967), with low-Ti–Zr subprovinces dominating overall and high-Ti–Zr basalts widespread in northern Botswana, Zimbabwe (Jones *et al.*, 2001), the Tuli syncline and the northern Lebombo (Duncan *et al.*, 1990; Sweeney *et al.*, 1994). Outside of the Karoo magmatic province, coeval high-Ti basalts crop out in the Falkland Islands (Mitchell *et al.*, 1999) and the Ahlmannryggen region of western Dronning Maud Land (Harris *et al.*, 1990; Riley *et al.*, 2005).

The Ferrar magmatic province extends over 3500 km from the Theron Mountains of Antarctica (Fig. 1) to SE Australia and Tasmania. The volume of the entire province is relatively small (<500 000 km^3) compared with other large igneous provinces (typically >10^6 km^3) and a significant part of this volume is contained in the Dufek–Forrestal layered mafic intrusion (Fleming *et al.*, 1997). The basalts of the Ferrar province are entirely of the low-Ti–Zr type and are typically high SiO_2 compared with Karoo compositions. The linear outcrop pattern (Fig. 1) of the Ferrar magmatic province is sub-parallel to the proto-Pacific margin of Gondwana, which has led some workers (e.g. Hergt *et al.*, 1991) to attribute the chemistry of the Ferrar magmas to enrichment of their mantle source by subduction-derived fluids. Cox (1988), however, attributed the linear outcrop pattern to a similar-shaped heat source (a hot line). Elliot *et al.* (1999) suggested the Ferrar magmas originated from a unique focus and that the present-day outcrop is the result of long distance magma transport from this point source. They suggested that magma transport was ultimately controlled by an active rift system initiated in the Early Jurassic and that the point source for the magmas was a thermal anomaly at the Weddell Sea triple junction (Fig. 1c) (Elliot & Fleming, 2000), which was also adjudged to be responsible for the Karoo low-Ti basalts of southern Africa.

The synchroneity of the Ferrar and Karoo provinces is well recognized (e.g. Encarnación *et al.*, 1996; Pálfy & Smith, 2000) as a result of detailed ^{40}Ar–^{39}Ar and U–Pb geochronology. A recent compilation of Karoo–Ferrar high-precision age determinations corrected to a common standard and common monitor age (Riley & Knight, 2001) confirm an overlap between the Karoo and Ferrar provinces, although the Karoo peak of 183 ± 2 Ma is ~3 Myr older than the Ferrar peak of 180·3 ± 2·2 Ma.

Underberg dykes

A suite of dykes that trends approximately NW–SE and crops out in the southern KwaZulu-Natal Province of SE Africa (Fig. 2), near the town of Underberg, has received very little attention. This dyke suite extends SE from the Karoo central area of Lesotho toward the coast (Fig. 2). The dykes are fine- to medium-grained dolerites and occur as rubbly outcrops, with coarser-grained weathered centres and finer-grained, sometimes glassy, intact margins. The dykes are typically >8 m width, with three dykes >45 m width, forming a clear bimodal population (Fig. 3a). Across the region, the dykes have a very uniform trend, with a strike orientation in the range 130–140° (Fig. 3b). This is different from the Okavango and southern Botswana dyke swarms, which trend consistently 110–120°. The Underberg dykes intrude sedimentary sequences of the Triassic Beaufort Group and the overlying Stormberg Group (Molteno, Elliot, Clarens formations), which consist of fine- to medium-grained sandstones, shales and mudstones (Turner, 1999). The Beaufort Group is overlain by the Molteno Formation, which consists of coarse, blue–grey sandstones. The overlying Elliot Formation consists of fine-grained red or purple shales and mudstones. The Early Jurassic Clarens Formation lies above the Elliot Formation and is made up of fine-grained cream sandstones.

The emplacement style of Karoo intrusions varies with stratigraphic height through the sedimentary sequence. At the base, thin sills dominate in the Dwyka and Ecca groups. Sills and sheets reach their maximum development in thickness and abundance within the Beaufort Group and are frequently transgressive and basin-shaped (Chevallier & Woodford, 1999). Cross-cutting dykes are also present in the Beaufort Group, but become more prominent in the overlying Molteno, Elliot and Clarens formations, which form the upper part of the sedimentary sequence.

Petrography

The dolerite dykes of the Underberg region are typically fine to medium grained and are feldspar-phyric. Rare phenocrysts of augite and unaltered olivine can also be identified in hand specimen. The plagioclase

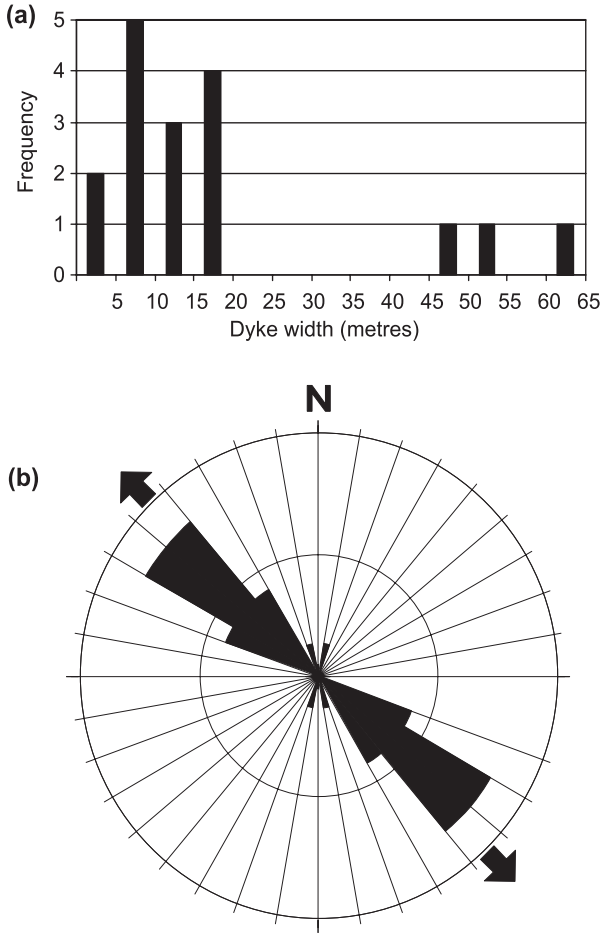

Fig. 3. (a) Frequency width diagrams and (b) frequency strike plots for the Underberg dykes.

phenocrysts are set in a groundmass of smaller plagioclase, augite and Fe–Ti oxides. The dykes typically have an intergranular and/or subophitic texture involving euhedral plagioclase laths and anhedral or equant augite crystals. At least two-thirds of the samples contain olivine, which in most cases is altered or corroded, although relatively fresh cores are preserved in some cases and some grains retain their euhedral habit. Olivine replacement minerals include iddingsite, carbonate and serpentine.

Sample numbering

Sample stations all have the prefix of SA. (e.g. SA.13). Samples from the same locality collected for geochemistry have the suffix .1 (e.g. SA.13.1), whereas samples for anisotropy of magnetic susceptibility (AMS) have the suffix .2 (e.g. SA.13.2), or .3, if two margins of the dyke were sampled. The grid reference (latitude–longitude) is the same for all samples from the same locality.

GEOCHRONOLOGY

Previous studies

Karoo volcanic province

Early geochronology studies of the mafic lavas and sills from the Karoo Province largely relied upon whole-rock K–Ar and Rb–Sr data (e.g. Allsopp *et al.*, 1984; Fitch & Miller, 1984). The K–Ar whole-rock method is now known to produce widely inaccurate results for volcanic rocks that have undergone even low-grade metamorphism (Walker & McDougall, 1982).

More recently, geochronology studies have been carried out using the $^{40}Ar/^{39}Ar$ and U–Pb methods. Duncan *et al.* (1997) reported a detailed $^{40}Ar/^{39}Ar$ incremental heating study of 32 mafic and silicic volcanic rocks (plagioclase mineral separates and whole-rock cores) from South Africa, Namibia and Antarctica. A 2 km lava succession in Lesotho yielded a close grouping of ages, such that the entire section was adjudged to have been erupted within ~0·5 Myr at ~183 Ma. Basaltic and rhyolitic volcanic rocks from the Lebombo–Mwenezi region have revealed a slightly broader age range, with two rhyolites yielding ages of 178·1 ± 0·6 and 179·7 ± 0·7 Ma and several mafic rocks giving ages between 181·2 ± 1·0 and 184·2 ± 0·6 Ma. Mafic sills, lavas, and dykes have also been analysed from the Marienthal area of Namibia, central and eastern South Africa, and KwaZulu-Natal, all of which yielded ages indistinguishable from the main period of Lesotho and Lebombo volcanism, ~182 ± 1 Ma. Recent work by Riley *et al.* (2004) on the U–Pb (sensitive high-resolution ion microprobe; SHRIMP) geochronology of rhyolites from the Lebombo has improved the dating of this area. This work, combined with the existing $^{40}Ar/^{39}Ar$ data, indicates that the 12 km succession of volcanic rocks in the Lebombo rift was erupted in 1–2 Myr at ~182 Ma.

The Okavango dyke swarm (Fig. 1) has been dated [$^{40}Ar/^{39}Ar$ (whole-rock and plagioclase) geochronology] by Elburg & Goldberg (2000) and Le Gall *et al.* (2002), who have suggested an emplacement age of 178–179 Ma.

Ferrar magmatic province

Dating of the Ferrar magmatic province of East Antarctica has previously yielded a broad spread of ages (90–308 Ma; Elliot *et al.*, 1985), although a 'preferred' age of 180 ± 5 Ma has been advocated as the best estimate (Elliot *et al.*, 1985). Recent, high-precision ages for magmatic rocks of the Ferrar province also demonstrate a short-lived episode of magmatism. Heimann *et al.* (1994) determined $^{40}Ar/^{39}Ar$ ages in the range 176·4 ± 0·6 to 177·2 ± 0·5 Ma from different stratigraphical levels within the Kirkpatrick basalts. Very similar ages were reported by Elliot *et al.* (1999), in the range 174·9 ± 0·5 to 177·4 ± 0·5 Ma, for a number of sills along the Transantarctic Mountains.

Table 1: Summary of $^{40}Ar/^{39}Ar$ radiometric ages for dykes from southern KwaZulu-Natal

Sample	Material	Total fusion age (Ma)	2σ error	Plateau age (Ma)	2σ error	N	MSWD	Isochron age (Ma)	2σ error	$^{40}Ar/^{36}Ar$ initial	2σ error	*J*
SA.3.1	feldspar	174·74	1·00	176·36	1·23	4/9	1·92	176·08	4·36	307·1	184·4	0·001540
SA.7.1	feldspar	176·11	0·94	176·13	1·17	4/7	2·18	177·11	1·20	257·6	50·6	0·001563
SA.19.1	whole rock	178·64	0·59	181·72	0·67	4/11	0·17	181·53	0·97	285·1	32·4	0·001750
SA.19.1				175·30	1·20	5/11	4·00	172·09	2·19	427·8	63·9	

Encarnación *et al.* (1996) used U–Pb geochronology on zircon and baddeleyite to determine the age of dolerite sills from the central Transantarctic Mountains and Victoria Land (Fig. 1), which yielded ages of 183·4 ± 1·4 and 183·8 ± 1·6 Ma, respectively. $^{40}Ar/^{39}Ar$ geochronology by Fleming *et al.* (1997) on feldspar and biotite separates from five dolerite sills yielded a range of plateau and total gas ages from 179·4 ± 0·7 to 181·0 ± 0·7 Ma. The age of emplacement of the Dufek Intrusion (Fig. 1) has been determined using U–Pb techniques on zircon separates (Minor & Mukasa, 1997), which gave crystallization ages of 182·7 ± 0·4 and 183·9 ± 0·4 Ma for a felsic dyke from the Dufek Massif and a capping granophyre intrusion, respectively.

Many of the recently published ages from the Karoo and Ferrar provinces were recalculated by Riley & Knight (2001) using a common neutron fluence monitor (MMhb-1) and a common age for that monitor (523·1 ± 2·6 Ma; Renne *et al.*, 1998). Most ages changed very little (<1 Myr) when recalculated, with the exception of the $^{40}Ar/^{39}Ar$ ages of the Ferrar intrusive and volcanic rocks produced by the Ohio State University laboratory (Heimann *et al.*, 1994; Fleming *et al.*, 1997; Elliot *et al.*, 1999). The published data from these workers yielded ages of ~176–177 Ma, using the neutron fluence monitor, MON-4 and an assigned age for MMhb-1 of 513·5 Ma. These ages were recalculated by Riley & Knight (2001) to ~180–181 Ma, which makes them consistent with other $^{40}Ar/^{39}Ar$ ages and U–Pb data.

Underberg dykes

There are no reported ages for the dyke suite near Underberg (Fig. 2), although Fitch & Miller (1984) reported both K–Ar and $^{40}Ar/^{39}Ar$ ages for several dykes that intrude the Lesotho Formation lavas at Monontsha Pass in NE Lesotho (Fig. 1). Based on dyke strike these dykes may well be a continuation of the Underberg dyke suite and yielded ages in the range 159–210 Ma, with preferred ages quoted at 159, 165 and 193 Ma for three olivine-bearing dykes. Encarnación *et al.* (1996) have dated (U–Pb) a granophyre from the New Amalfi sheet (Fig. 1) at 183·7 ± 0·6 Ma. The sheet is believed to be related to the Lesotho lavas and is fed by the Elephant's Head dyke, which crosscuts the lowermost lavas of the Lesotho lavas and is subparallel to the Underberg dykes.

This study

Three samples (SA.3.1, SA.7.1, SA.19.1) were selected for $^{40}Ar/^{39}Ar$ geochronology from across the Underberg region, providing the best possible spread based on the range of geochemical compositions.

Analytical methods

Samples were either 5 mm diameter whole-rock cores or copper-foil wrapped mineral separates, packaged in evacuated quartz vials, and were irradiated in the Oregon State University TRIGA Reactor for 6 h at 1 MW power on May 23, 2003. The neutron flux was measured using standard FCT-3 biotite, 28·03 Ma (Renne *et al.*, 1994). Reactor temperatures can reach 270°C. Additionally, samples were baked at 195°C for 48 h during extraction line pump-down to $\sim 10^{-9}$ torr.

Depending on sample composition, the incremental heating experiment started in the range 400–600°C and was typically complete by 1400°C, using a Heine low-blank resistance furnace with a Ta–Nb crucible and Mo liner. Each heating step was of 20 min duration with an additional 5 min cooling and continued removal of active gases with St101 Zr–Al and St172 Zr–V–Fe getters.

A MAP 215-50 rare gas mass spectrometer source at 3000 V, and equipped with a Johnston MM1-1SG electron multiplier at 2050 V, was used for analysis. During the 15 min analysis time per mass peak height, data were collected for 10 cycles of masses 35–40 for baselines and peak tops. Data were reduced and age calculations completed using ArArCALC v2.2 software for $^{40}Ar/^{39}Ar$ geochronology (Koppers, 2002).

Results

The $^{40}Ar/^{39}Ar$ results are presented in Table 1 and Fig. 4. Plagioclase separated from sample SA.3.1 yielded an

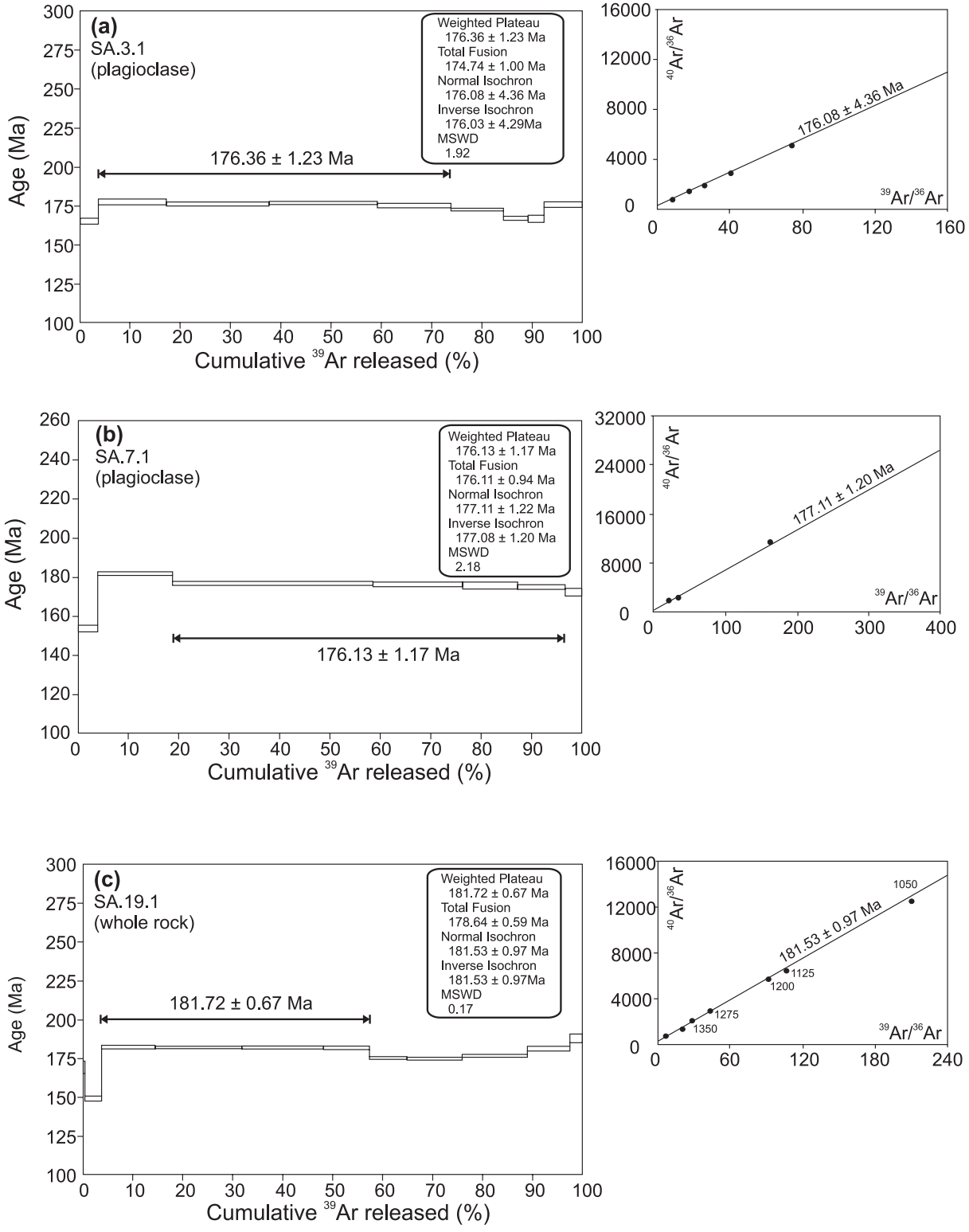

Fig. 4. The ^{39}Ar release spectra for samples SA.3.1, SA.7.1 and SA.19.1. All three samples generate plateaux and satisfy the criteria of three release steps comprising 50% of the total release. Also shown are the isochron diagrams for the three samples. For sample SA.19.1, the numbers next to five points in the isochron are the highest temperature steps (numbers are°C), which are collinear and define an isochron somewhat younger (173 Ma) than the isochron shown by steps 3–6 (181 Ma). The intercept (^{40}Ar/^{36}Ar) is significantly above the atmospheric composition, indicating initial excess Ar, so two interpretations are possible.

excellent mid-temperature, four-step plateau (176·4 ± 1·2 Ma; Fig. 4a) comprising 70% of total gas released, which is the preferred age. There is slight ^{40}Ar loss (first step only) and ^{39}Ar recoil at high temperature. The isochron is concordant at 176·1 ± 4·4 Ma. Plagioclase separated from sample SA.7.1 also yielded an excellent mid- to high-temperature plateau (176·1 ± 1·2 Ma; Fig. 4b) comprising 78% of gas released, which is the preferred age. Again there is slight ^{40}Ar loss (first step only) and ^{39}Ar recoil (step 2). The isochron is concordant at 177·1 ± 1·2 Ma. Whole-rock sample SA.19.1 provided a good low- to mid-temperature, four-step plateau (181·7 ± 0·7 Ma; Fig. 4c) comprising 54% of total gas released. There is evidence of ^{40}Ar loss at low temperature and ^{39}Ar recoil at high temperature. There is a 'secondary' plateau (steps 7–9) that gives a mean age of 175·3 ± 1·2 Ma. The corresponding isochron for these high-temperature steps is 172·1 ± 2·2 Ma, and an initial $^{40}Ar/^{36}Ar$ ratio of 428 (distinct from the atmospheric value of 296). There is therefore a possibility that this dyke contains excess ^{40}Ar, which may be responsible for the older step ages. On this basis, SA.19.1 could be contemporaneous with SA.3.1 and SA.7.1.

WHOLE-ROCK GEOCHEMISTRY OF DYKES

Analytical techniques

Powders for geochemical analysis were prepared from 2–3 kg of fresh rock. Samples were reduced to pass a 1700 μm sieve using a hardened steel fly press. The powders were produced using an agate Tema-mill. Sr and Nd isotope compositions were measured at the NERC Isotope Geosciences Laboratory (Keyworth, UK) on a Finnigan-MAT 262 mass spectrometer. Rb–Sr and Sm–Nd analysis followed procedures described by Pankhurst & Rapela (1995). Sr isotope composition was determined in multidynamic peak-jumping mode. During the period of analysis, 22 analyses of the Sr isotope standard NBS987 gave a value of 0·710259 ± 0·000008 (2σ errors). Nd-isotope composition was determined in static collection mode. Twenty-four analyses of the in-house J&M Nd isotope standard gave a value of 0·511196 ± 0·000022 (2σ errors); reported $^{143}Nd/^{144}Nd$ values were normalized to a value of 0·511130 for this standard, equivalent to 0·511864 for La Jolla.

Major and selected trace element whole-rock analysis was by standard X-ray fluorescence (XRF) techniques at the Department of Geology, University of Keele, following the methods described by Floyd (1985). Higher precision trace element abundances were determined by inductively coupled plasma mass spectrometry (ICP-MS) at the University of Durham. The analytical methods, precision, and detection limits have been detailed by Ottley *et al.* (2003).

Classification

The major and trace element and Sr–Nd isotope data are reported in Table 2. The analysed samples are subalkaline and range in composition from basalt to basaltic andesite (Fig. 5) and on the basis of their CIPW norms (Yoder & Tilley, 1962) they can all be classified as quartz tholeiites (Table 2), although two samples (SA.19.1, SA.20.1) are on the boundary between quartz and olivine tholeiites. When the data for the Underberg dykes are plotted against MgO (wt %) as an index of differentiation (Fig. 6), Ni is strongly correlated with MgO, suggesting olivine control during magmatic differentiation. Al_2O_3 increases as MgO decreases, suggesting that plagioclase fractionation is not important until MgO contents fall below ~7 wt %. Many of the major and trace elements exhibit compositional trends typical of tholeiites, with negative correlations of Fe_2O_3, TiO_2, Zr and Y with MgO (Fig. 6).

In common with other studies of Mesozoic and older flood basalt provinces we primarily use the incompatible high field strength elements (HFSE; Ti, Zr, Y, Nb) as discriminants between magma types. These elements are considered largely immobile during low-temperature alteration processes (e.g. Peate, 1997) and ratios between them are not significantly modified by moderate amounts of fractional crystallization or susceptible to variations in the degree of partial melting (e.g. Luttinen & Furnes, 2000). Zr can be used as an effective index of differentiation in magmas that do not crystallize zircon. These discriminants are subsequently supported by variations in $^{87}Sr/^{86}Sr$, $^{143}Nd/^{144}Nd$, rare earth element (REE) and other major and trace elements and their ratios.

The Underberg dykes are all low-Ti–Zr (LTZ) tholeiites with TiO_2 <1·5 wt % and Zr <150 ppm (Fig. 7), consistent with Sweeney *et al.*'s (1994) classification of a Karoo low-Ti magma type. Geochemically they overlap with the majority of low-Ti basalt types of the Karoo, including the once-contiguous Dronning Maud Land (Fig. 1) lavas from Kirwanveggen, Heimefrontfjella and Vestfjella (Harris *et al.*, 1990; Luttinen & Furnes, 2000). They also overlap with the principal field of Ferrar tholeiites (Antonini *et al.*, 1999). The Underberg dykes have SiO_2 contents in the range 48·8–54·5 wt % and have typically low Mg numbers (48·9–68·8; mean of 55·4; Table 2).

Cr and Ni contents are varied (Cr 125–837 ppm; Ni 49–267 ppm). The Underberg dykes are all light REE (LREE) enriched, with $(La/Lu)_N$ ranging from 2·2 to 5·3, and typically have flat middle REE (MREE) to heavy REE (HREE) chondrite-normalized patterns (Fig. 8).

Table 2: Whole-rock analyses of dolerite dykes from southern KwaZulu-Natal (South Africa)

Sample:	SA.2.1	SA.3.1	SA.4.1	SA.5.1	SA.6.1	SA.7.1	SA.9.1	SA.10.1	SA.11.1
Latitude (S):	29·5740	29·5846	29·5822	29·6514	29·6543	29·8394	29·9359	29·8998	29·8686
Longitude (E):	29·5978	29·6147	29·6274	29·5956	29·5475	29·5161	29·4875	29·5588	29·6059
Altitude (m):	1447	1389	1395	1436	1388	1416	1774	1551	1545
SiO_2	51·47	52·43	50·26	54·49	53·61	50·68	49·87	51·33	49·59
TiO_2	1·09	0·89	1·13	1·12	1·14	1·30	1·36	0·99	1·10
Al_2O_3	14·71	15·18	14·86	14·44	14·60	14·62	14·66	14·99	16·38
Fe_2O_3(T)	11·67	9·94	12·67	10·43	11·43	13·10	10·85	11·16	10·36
MnO	0·18	0·16	0·19	0·15	0·17	0·20	0·16	0·18	0·16
MgO	6·04	8·05	6·47	5·71	5·88	6·21	9·62	7·43	6·64
CaO	10·55	10·73	10·47	8·60	9·71	10·47	10·16	10·68	11·65
Na_2O	2·35	2·11	2·55	2·69	2·59	2·44	2·25	2·23	2·59
K_2O	0·57	0·56	0·76	0·88	0·70	0·74	0·49	0·52	0·71
P_2O_5	0·19	0·10	0·17	0·18	0·15	0·21	0·20	0·17	0·23
LOI	0·40	0·28	0·03	0·84	0·20	0·02	0·46	0·40	0·35
Total	99·23	100·44	99·56	99·53	100·17	99·99	100·08	100·08	99·78
mg-no.	51·5	62·4	51·1	52·9	51·3	49·3	64·5	57·7	56·8
Cr	143	397	130	129	152	139	703	282	274
Ni	50	90	57	55	65	54	182	78	84
Co	40·4	47·4	44·5	40·1	41·7	43·5	50·3	44·8	39·5
Ga	17·83	16·45	17·94	19·82	20·02	18·60	17·07	16·77	17·99
Rb	12·14	14·73	19·31	24·63	19·65	16·44	8·33	11·10	11·56
Sr	221·2	138·6	224·5	296·6	231·7	191·6	255·5	214·5	337·9
Y	27·9	24·6	28·8	27·5	28·3	33·7	23·5	28·1	23·9
Zr	108	81	104	121	113	124	95	94	92
Nb	8·41	2·88	5·84	7·14	4·92	7·49	4·35	5·77	14·41
Cs	1·03	0·39	0·38	0·98	0·36	0·35	1·55	1·05	0·39
Ba	207	190	232	367	310	237	184	188	187
La	11·1	8·1	10·6	18·7	12·8	12·2	7·9	9·4	11·9
Ce	23·7	17·6	22·9	37·4	26·9	26·3	17·8	20·5	24·6
Pr	3·29	2·49	3·20	4·78	3·64	3·69	2·63	2·87	3·33
Nd	14·9	11·3	14·4	19·7	16·1	16·8	12·4	13·1	14·7
Sm	3·55	2·92	3·68	4·49	4·13	4·19	3·25	3·30	3·42
Eu	1·16	0·89	1·14	1·34	1·26	1·29	1·16	1·08	1·21
Gd	4·35	3·67	4·48	5·08	4·88	5·14	3·86	4·09	4·02
Tb	0·732	0·650	0·760	0·823	0·816	0·878	0·639	0·699	0·665
Dy	4·46	3·96	4·76	4·77	4·82	5·36	3·86	4·38	3·94
Ho	0·96	0·85	1·00	0·96	0·97	1·16	0·81	0·95	0·82
Er	2·62	2·33	2·74	2·48	2·54	3·20	2·18	2·62	2·20
Tm	0·408	0·362	0·428	0·374	0·377	0·497	0·331	0·400	0·330
Yb	2·60	2·30	2·78	2·29	2·37	3·19	2·12	2·59	2·12
Lu	0·43	0·38	0·46	0·36	0·37	0·52	0·34	0·43	0·34
Hf	2·68	2·17	2·68	3·04	2·93	3·15	2·41	2·40	2·19
Ta	0·503	0·234	0·389	0·442	0·345	0·454	0·310	0·370	0·813
Pb	2·78	3·44	3·15	5·38	4·83	3·81	2·61	2·77	1·32
Th	1·45	1·81	1·62	3·12	2·81	1·80	0·73	1·28	1·24
U	0·31	0·23	0·34	0·69	0·62	0·38	0·15	0·29	0·31
Rb	12·1	14·7	19·3	24·6	19·7	16·4	8·3		11·56
Sr	221·2	138·6	224·5	296·6	231·7	191·6	255·5		337·9

Table 2: Continued

Sample:	SA.2.1	SA.3.1	SA.4.1	SA.5.1	SA.6.1	SA.7.1	SA.9.1	SA.10.1	SA.11.1
Latitude (S):	29·5740	29·5846	29·5822	29·6514	29·6543	29·8394	29·9359	29·8998	29·8686
Longitude (E):	29·5978	29·6147	29·6274	29·5956	29·5475	29·5161	29·4875	29·5588	29·6059
Altitude (m):	1447	1389	1395	1436	1388	1416	1774	1551	1545
$^{87}Rb/^{86}Sr$	0·158711	0·307657	0·248803	0·240327	0·245441	0·248288	0·094296		0·098982
$^{87}Sr/^{86}Sr_m$	0·706150	0·709748	0·707915	0·710585	0·710625	0·706828	0·705543		0·704757
$^{87}Sr/^{86}Sr_{180}$	0·705744	0·708961	0·707278	0·709970	0·709997	0·706193	0·705302		0·704504
Sm	3·75	2·89	3·65	4·52	4·24	5·69	3·45		3·39
Nd	14·64	10·64	13·79	19·04	15·97	21·64	12·57		13·811
$^{147}Sm/^{144}Nd$	0·1549	0·1642	0·1599	0·1434	0·1605	0·1590	0·1660		0·1484
$^{143}Nd/^{144}Nd_m$	0·512485	0·512406	0·512419	0·511834	0·512132	0·512467	0·512483		0·512628
εNd_{180}	−2·0	−3·8	−3·4	−14·5	−9·0	−2·5	−2·3		0·9
Age	176·4 + 1·2				176·1 + 1·2				

Sample:	SA.12.1	SA.13.1	SA.14.1	SA.15.1	SA.16.1	SA.17.1	SA.18.1	SA.19.1	SA.20.1
Latitude (S):	29·7875	29·8577	29·8587	29·9528	30·0117	30·0339	30·0895	30·1562	30·2402
Longitude (E):	29·4537	29·4324	29·4345	29·3574	29·3520	29·3498	29·3302	29·2392	29·3275
Altitude (m):	1530	1763	1775	1574	1676	1861	1803	1759	1579
SiO_2	50·82	50·11	52·52	52·55	51·92	51·97	51·84	48·81	49·51
TiO_2	1·29	1·25	1·12	1·12	1·10	1·06	1·18	1·10	0·85
Al_2O_3	14·59	15·87	14·05	13·95	14·15	14·07	14·19	14·03	13·93
$Fe_2O_3(T)$	13·14	11·09	12·11	12·15	12·58	11·07	12·42	11·87	10·40
MnO	0·19	0·18	0·18	0·18	0·19	0·17	0·19	0·18	0·16
MgO	6·13	6·26	6·12	6·28	6·28	7·43	6·56	11·12	11·18
CaO	10·20	11·23	10·54	10·50	10·81	10·43	10·43	10·68	11·35
Na_2O	2·43	2·60	2·26	2·34	2·29	2·29	2·45	2·11	1·95
K_2O	1·00	0·53	0·62	0·65	0·64	0·57	0·58	0·42	0·34
P_2O_5	0·21	0·26	0·16	0·19	0·16	0·15	0·19	0·21	0·16
LOI	0·06	0·58	0·03	0·25	0·10	0·54	0·22	−0·18	0·11
Total	100·07	99·94	99·72	100·16	100·22	99·75	100·26	100·34	99·93
mg-no.	48·9	53·6	50·9	51·4	50·6	57·9	52·0	65·8	68·8
Cr	143	227	128	227	125	332	238	730	837
Ni	49	80	58	51	60	87	53	256	267
Co	42·8	38·9	45·4	44·1	45·6	45·8	43·3	57·7	57·2
Ga	18·26	18·44	18·07	18·04	17·90	16·87	17·76	16·21	15·44
Rb	20·58	10·20	15·51	12·69	14·43	11·83	12·44	7·84	6·80
Sr	241·5	318·8	200·4	214·6	200·3	210·4	222·7	249·8	255·7
Y	33·0	26·8	29·2	30·5	29·2	25·2	30·6	21·7	17·7
Zr	123	105	104	118	104	82	116	81	62
Nb	7·41	16·67	5·84	8·40	5·79	7·34	7·50	7·80	5·90
Cs	0·40	2·04	0·62	0·36	0·63	1·01	0·36	0·78	0·44
Ba	688	191	199	217	199	188	291	178	207
La	11·7	13·7	10·3	12·3	10·2	8·6	11·9	7·6	5·9
Ce	25·5	28·4	22·3	26·0	22·2	18·2	25·7	17·4	13·5
Pr	3·55	3·79	3·11	3·59	3·11	2·54	3·56	2·56	1·99
Nd	16·1	16·6	14·1	15·9	14·1	11·6	16·0	12·2	9·5
Sm	4·05	3·83	3·61	3·83	3·61	3·02	3·96	3·14	2·51
Eu	1·27	1·33	1·14	1·19	1·13	1·04	1·19	1·11	0·91

Sample:	SA.12.1	SA.13.1	SA.14.1	SA.15.1	SA.16.1	SA.17.1	SA.18.1	SA.19.1	SA.20.1
Latitude (S):	29·7875	29·8577	29·8587	29·9528	30·0117	30·0339	30·0895	30·1562	30·2402
Longitude (E):	29·4537	29·4324	29·4345	29·3574	29·3520	29·3498	29·3302	29·2392	29·3275
Altitude (m):	1530	1763	1775	1574	1676	1861	1803	1759	1579
Gd	5·06	4·53	4·39	4·60	4·43	3·80	4·69	3·87	3·05
Tb	0·853	0·745	0·755	0·788	0·755	0·654	0·792	0·619	0·500
Dy	5·20	4·44	4·67	4·76	4·60	3·99	4·85	3·56	2·90
Ho	1·13	0·93	0·99	1·02	1·00	0·86	1·05	0·74	0·60
Er	3·10	2·48	2·73	2·82	2·73	2·37	2·85	1·97	1·60
Tm	0·483	0·377	0·418	0·438	0·426	0·368	0·441	0·295	0·238
Yb	3·14	2·39	2·73	2·86	2·71	2·35	2·85	1·88	1·51
Lu	0·51	0·38	0·44	0·47	0·45	0·37	0·47	0·30	0·24
Hf	3·11	2·53	2·63	2·96	2·67	2·11	2·96	2·04	1·60
Ta	0·447	0·904	0·371	0·482	0·376	0·426	0·425	0·436	0·362
Pb	3·34	1·77	3·29	3·59	3·06	2·45	3·55	1·65	1·28
Th	1·74	1·43	1·59	1·71	1·59	1·19	1·77	0·73	0·59
U	0·37	0·34	0·33	0·36	0·33	0·27	0·33	0·19	0·15
Rb	20·58	10·20		12·69	14·43	11·83	12·44	7·84	6·80
Sr	241·5	318·8		214·6	200·3	210·4	222·7	249·8	255·7
$^{87}Rb/^{86}Sr$	0·246587	0·092544		0·170990	0·208460	0·162693	0·161630	0·090794	0·076940
$^{87}Sr/^{86}Sr_m$	0·708114	0·704784		0·706974	0·707349	0·705952	0·707005	0·704655	0·704804
$^{87}Sr/^{86}Sr_{180}$	0·707483	0·704547		0·706536	0·706816	0·705536	0·706591	0·704423	0·704607
Sm	3·98	3·95		3·79	3·60	3·04	3·92	2·67	3·43
Nd	15·10	16·08		14·95	13·56	11·21	15·28	9·54	12·41
$^{147}Sm/^{144}Nd$	0·1593	0·1486		0·1531	0·1604	0·1638	0·1549	0·1689	0·1671
$^{143}Nd/^{144}Nd_m$	0·512463	0·512637		0·512419	0·512418	0·512553	0·512441	0·512570	0·512560
εNd_{180}	−2·6	1·1		−3·3	−3·5	−0·9	−2·9	−0·7	−0·8
Age								181·7 + 0·7	

m, measured.

Most samples have a distinctive negative Eu-anomaly as a result of plagioclase fractionation. The multi-element variations in Fig. 9 are characterized by distinct troughs at Ta–Nb, P and Ti, when normalized to primitive mantle; however, four samples (SA.11.1, SA.13.1, SA.19.1, SA.20.1; dashed lines in Fig. 9) have flatter multi-element patterns with no marked troughs at Ta–Nb and P.

The Underberg dykes show a significant range of variation in a diagram of Th/Yb vs Nb/Yb (Fig. 10) where they are plotted relative to the mid-ocean ridge basalt (MORB)–ocean island basalt (OIB) mantle array and compared with a restricted (because of a lack of good Th data) range of Karoo and Ferrar dolerites. The majority of the Underberg dykes plot toward the low-Ti field of the Vestfjella lavas. Four samples (SA.11.1, SA.13.1, SA.19.1, SA.20.1) plot within the MORB–OIB array, which are the same four samples with no marked Nb–Ta anomaly (Fig. 7). The remaining samples trend toward higher Th/Yb values, indicating an increased contribution from continental crust and/or partial melts of subduction-modified lithosphere. Three samples (SA.3.1, SA.5.1, SA.6.1) plot toward even higher Th/Yb values, and have amongst the highest SiO_2 contents and are isotopically 'Ferrar-like'. They plot close to the Ferrar field and also the field of average global subducting sediment (GLOSS).

Therefore, central to the discussion regarding the petrogenesis of the Underberg dyke suite is resolving the contributions from the continental crust and a lithospheric mantle source enriched by subduction-derived fluids.

The Underberg dykes display significant variations in both $^{87}Sr/^{86}Sr$ and εNd (at 180 Ma). $^{87}Sr/^{86}Sr$ varies from 0·7044 to 0·7090, whereas εNd_i varies from −3·8 to 1·1 (Fig. 11). The two samples with positive εNd_i values (SA.11.1 and SA.13.1) also have the least radiogenic initial $^{87}Sr/^{86}Sr$ values (0·7045) and plot within the OIB array (Fig. 10). The two other samples which plot in the

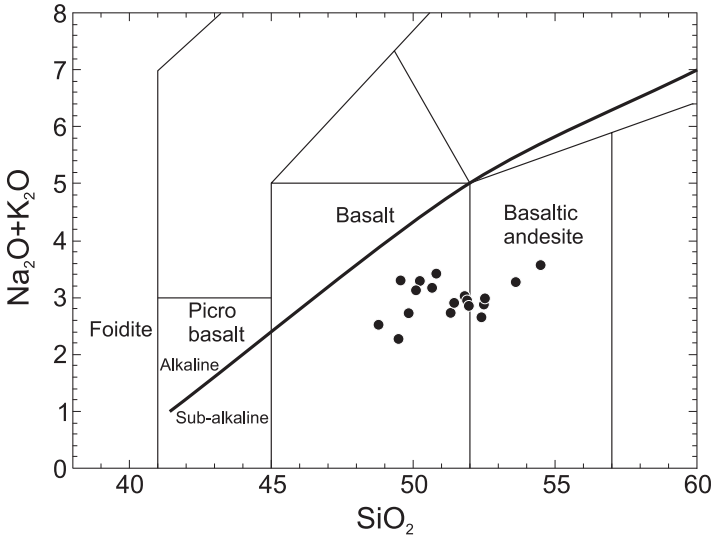

Fig. 5. Total alkali vs SiO_2 diagram (wt %) for the Underberg dyke suite. The samples are basalt or basaltic andesite and are all classified as quartz tholeiites based on their CIPW norms. Classification boundaries are from Le Bas *et al.* (1986). Data from Table 2.

OIB array (Fig. 10) have very similar $^{87}Sr/^{86}Sr$ values (0·7044–0·7046), but have marginally negative εNd_i values (−0·7 to −0·8). Rocks with positive εNd values are rare in the Karoo volcanic province and are absent from the Ferrar magmatic province. Dykes of the Rooi Rand (Duncan *et al.*, 1990), central Lebombo (Sweeney *et al.*, 1994), Falkland Islands (east–west trending; Mitchell *et al.*, 1999), Ahlmannryggen, Dronning Maud Land (Riley *et al.*, 2005) and rare rocks from Vestfjella (Luttinen & Furnes, 2000) and Kirwanveggen (Harris *et al.*, 1990) also have positive εNd, with the Ahlmannryggen Group 3 dykes (Riley *et al.*, 2005) being the most depleted (MORB-like with $\varepsilon Nd_i \sim +9$) in the entire Karoo volcanic province.

DISCUSSION

The key questions concerning the petrogenesis of almost all continental flood basalt (CFB) magma types are centred on the relative contributions from sub-lithospheric mantle sources (mantle plume, ambient asthenosphere), lithospheric mantle and continental crust. Low-Ti–Zr tholeiites are the predominant rock type throughout the Karoo volcanic province (e.g. Sweeney *et al.*, 1994; Marsh *et al.*, 1997). These are isotopically and elementally distinct from oceanic basalt compositions, which has led many workers to highlight the important role of the subcontinental lithospheric mantle (SCLM) in Karoo magma petrogenesis (e.g. Hawkesworth *et al.*, 1984, 1999; Ellam & Cox, 1991; Saunders *et al.*, 1992; Sweeney *et al.*, 1994).

The Ferrar magmatic province is geochemically distinct (high SiO_2, high $^{87}Sr/^{86}Sr$, low εNd) from the Karoo volcanic province, which has led to the interpretation that the Ferrar magmas either were extensively contaminated by the continental crust (Faure *et al.*, 1982; Antonini *et al.*, 1999) or were derived from an enriched lithospheric mantle source (Kyle, 1980; Hergt, 2000), where the enrichment was related to earlier subduction along the Gondwana margin. Although the Karoo and Ferrar magmatic provinces are broadly contemporaneous (Pálfy & Smith, 2000), they are generally regarded as being distinct provinces derived from separate magma sources. However, Elliot & Fleming (2000) have identified Ferrar-like lavas (Golden Gate) in the centre of the Karoo volcanic province, which led to the inevitable conclusion that the two provinces may overlap.

The multi-element patterns in Fig. 9 include four samples with relatively flat trends (dashed lines) compared with the remaining dykes, which are characterized by pronounced negative anomalies in Nb, Ta, P and Ti, typical of arc-related basalts. Puffer (2001) noted that some Karoo basalts (and other continental flood basalts) have arc-like trace element abundances, which can be attributed to the melting of pre-existing subduction-modified mantle.

Analysis of the geochemical and isotopic data indicates that the petrogenetic issues central to understanding the Underberg dykes are the role of crustal contamination, the modification of the lithospheric mantle by subduction-derived fluids and links to the Ferrar magmatic province.

Role of crustal contamination

Interaction between an ascending mafic magma and the surrounding continental crust is inevitable at some point

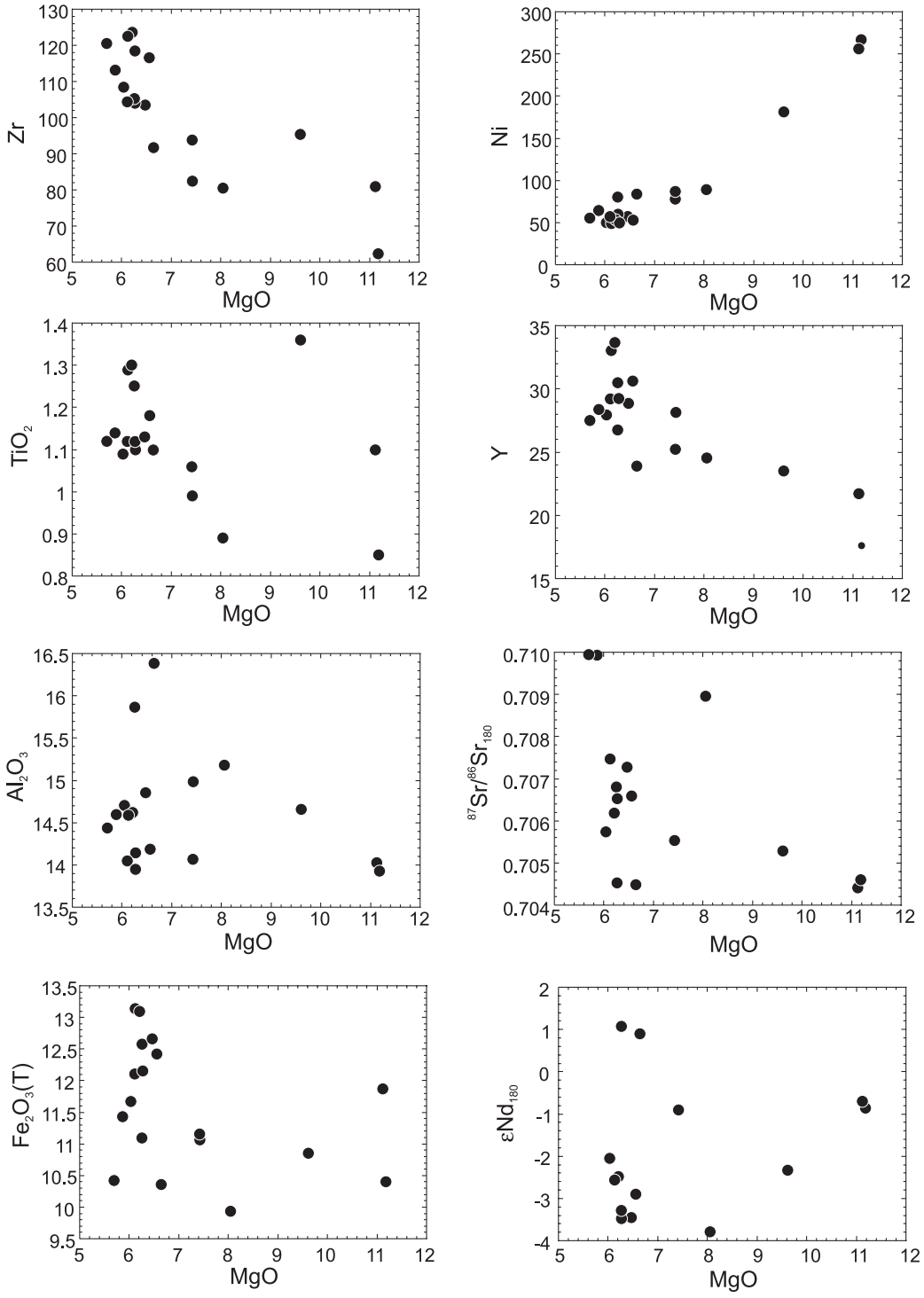

Fig. 6. Variations in Zr, TiO_2, Al_2O_3, Fe_2O_3, Ni, Y, $^{87}Sr/^{86}Sr_i$ and εNd_i vs MgO for the Underberg dyke suite.

prior to eruption or intrusion, although in some cases the chemical changes to the magma may be insignificant. Any attempts to model the effects of crustal contamination have to consider the varied composition of the local crust and the composition of the uncontaminated parent magma.

Potential proxies for the upper crust in the KwaZulu-Natal Province include the granitic basement of the

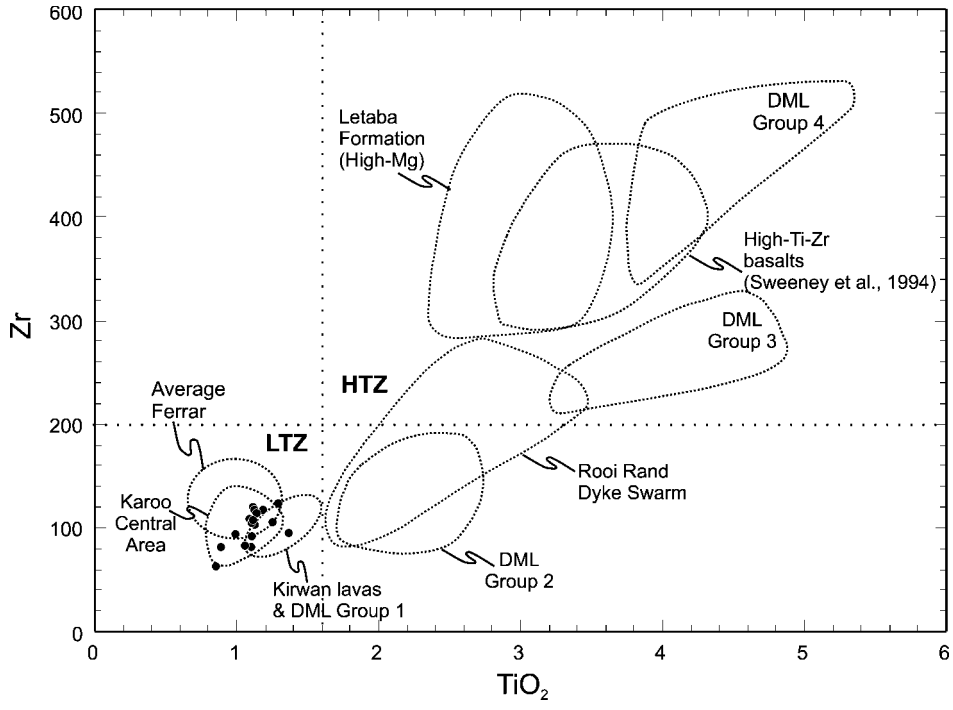

Fig. 7. Variation in Zr vs TiO_2 for KwaZulu-Natal dykes shown in comparison with dykes from the Ahlmannryggen (DML, groups 1–4; Riley *et al.*, 2005), Kirwan lavas (Harris *et al.*, 1990), Karoo central area (Marsh *et al.*, 1997), Rooi Rand dyke swarm (Duncan *et al.*, 1990) Letaba Formation, Lebombo HTZ basalts (Sweeney *et al.*, 1994), and average Ferrar (Antonini *et al.*, 1999).

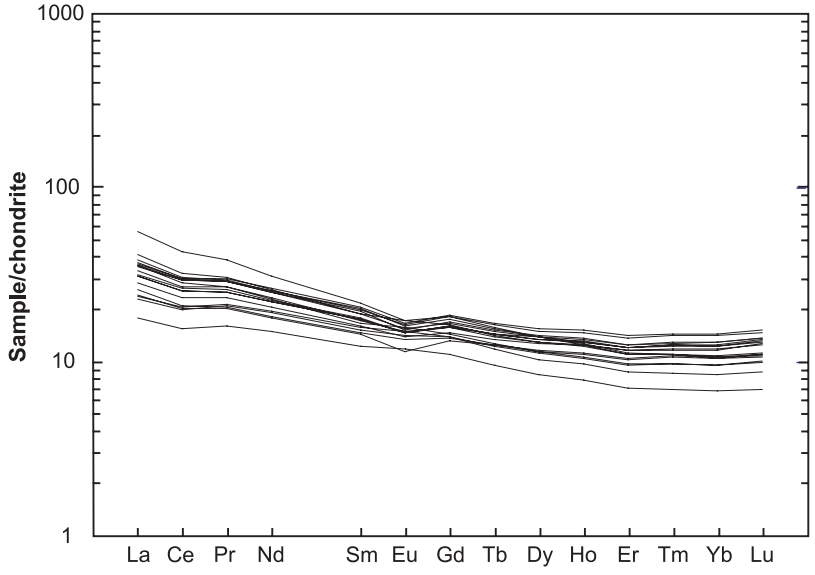

Fig. 8. Chondrite (Nakamura, 1974) normalized REE diagrams for Underberg dykes.

regionally extensive Mesoproterozoic Namaqua–Natal Belt or hornfels of the Ecca Group. Granitic basement of the Namaqua–Natal Belt has been sampled from deep boreholes (2·5 km). The granitic basement has negative εNd values (−4·4) and strongly radiogenic $^{87}Sr/^{86}Sr$ (0·7618) at 180 Ma (Eglington & Armstrong, 2003), and Ecca Group hornfels from the Insizwa intrusion has similar εNd values (−4·3) and $^{87}Sr/^{86}Sr$ values of 0·710 at 180 Ma (Lightfoot & Naldrett, 1984).

Potential primary magma compositions could include the most isotopically depleted rocks of the Underberg suite (e.g. SA.13.1; Table 2), which are akin to the Rooi

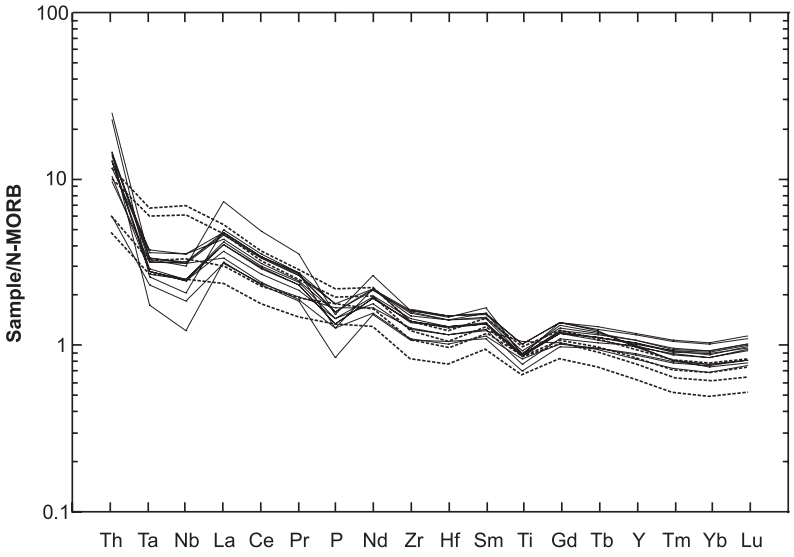

Fig. 9. N-MORB normalized incompatible element diagrams for the Underberg dykes. Four samples (SA.11.1, SA.13.1, SA.19.1, SA.20.1) are shown as dashed lines and are distinct from the other samples as they do not possess negative Ta, Nb and P anomalies. Normalizing values are taken from Sun & McDonough (1989).

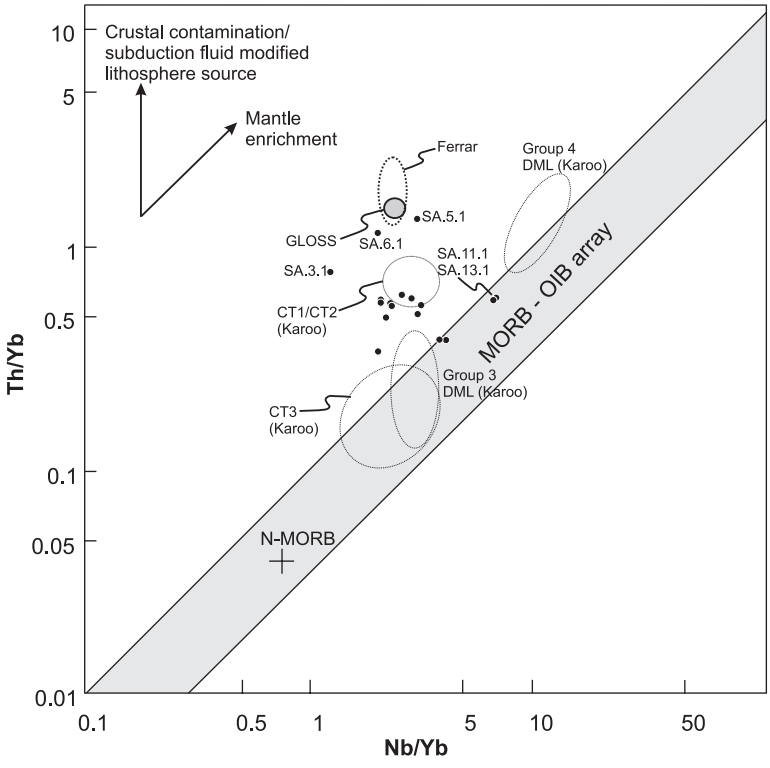

Fig. 10. Variations in Th/Yb vs Nb/Yb showing the composition of basic dykes from KwaZulu-Natal relative to the MORB–OIB array (Pearce & Peate, 1995). The DML fields are from the Ahlmannryggen (Riley *et al.*, 2005) and the CT1-3 fields are from Vestfjella (Luttinen & Furnes, 2000). Average Ferrar is from Molzahn *et al.* (1996) and GLOSS is average global subducting sediment from Plank & Langmuir (1998).

Rand dykes of the central Lebombo (Duncan *et al.*, 1990), considered to be amongst the most depleted rocks in the Karoo of South Africa. The most depleted rocks in the entire Karoo province are from the Dronning Maud Land region of Antarctica (Riley *et al.*, 2005). They have εNd values of +9, $^{87}Sr/^{86}Sr$ values close to 0·7035, and could also form a potential primary composition.

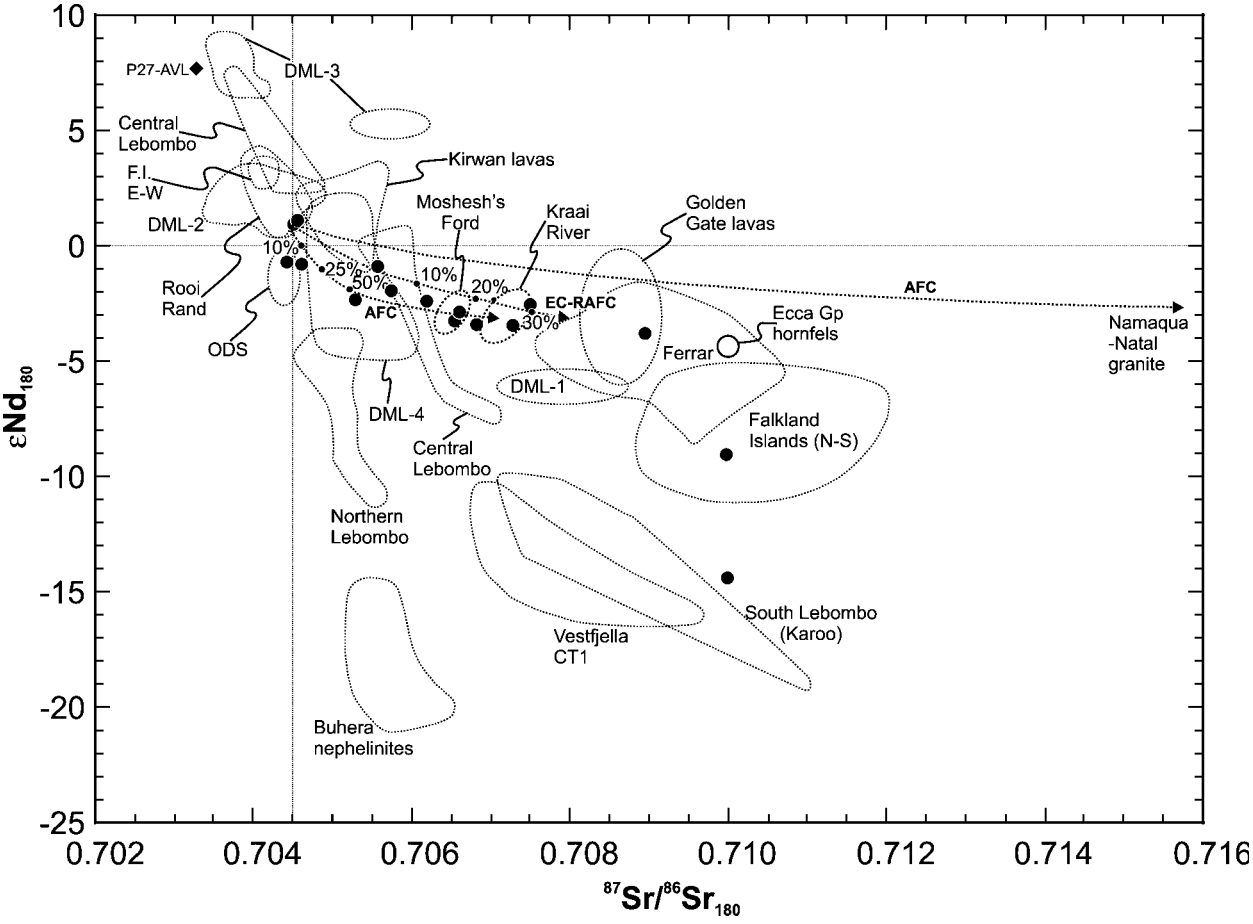

Fig. 11. Initial εNd and $^{87}Sr/^{86}Sr$ for KwaZulu-Natal dykes relative to fields from elsewhere in the Karoo and Ferrar magmatic provinces. Data sources: Duncan *et al.* (1990); Harris *et al.* (1990); Hergt *et al.* (1991); Sweeney *et al.* (1994); Fleming *et al.* (1997); Harmer *et al.* (1998); Antonini *et al.* (1999); Mitchell *et al.* (1999); Elburg & Goldberg (2000); Luttinen & Furnes (2000); Riley *et al.* (2005). ODS, Okavango dyke swarm; P27-AVL, depleted end-member from Luttinen & Furnes (2000); DML-1, 2, 3, 4, Dronning Maud Land geochemical groups 1–4; F.I., Falkland Islands. Two AFC curves are plotted; all use the same mantle-derived basalt end-member (Underberg dykes SA.11.1/SA.13.1; $^{87}Sr/^{86}Sr = 0{\cdot}7045$, εNd = 1·0, Sr 330 ppm, Nd 15 ppm) and two different crustal end-members (Namaqua–Natal granite: $^{87}Sr/^{86}Sr = 0{\cdot}7618$, εNd = −4·3, Sr 161 ppm, Nd 73 ppm; Ecca Group hornfels: $^{87}Sr/^{86}Sr = 0{\cdot}710$, εNd = −4·4, Sr 279 ppm, Nd 80 ppm). The third model curve is derived using the EC-RAFC model of Spera & Bohrson (2004) using the Ecca Group hornfels as the crustal end-member (Table 4).

Assimilation with fractional crystallization (AFC)

There is, in part, a weak correlation between $^{87}Sr/^{86}Sr_i$ and MgO (Fig. 6), suggesting that combined assimilation and fractional crystallization (AFC) could have affected some of the Underberg dykes. However, much of the variation in $^{87}Sr/^{86}Sr$ (∼0·7045–0·7075) occurs at fairly uniform MgO (∼6–6·6 wt %; Fig. 6), indicating that AFC was not the primary process ressponsible for the geochemical variation in the Underberg dykes; however, the remainder of the dykes do show co-variation in MgO and $^{87}Sr/^{86}Sr$ (Fig. 6), which could be accounted for by AFC processes. AFC was modelled for the Underberg dykes using the energy-constrained recharge–assimilation–fractional crystallization (EC-RAFC) model of Spera & Bohrson (2004), as well as the AFC equations of De Paolo (1981). EC-RAFC differs from standard AFC models in that it tracks the isotopic and trace element composition of the melt, cumulate, country rock partial melts and enclaves during simultaneous recharge, assimilation and fractional crystallization (Fowler *et al.*, 2004).

The depleted composition from Dronning Maud Land (Riley *et al.*, 2005) is an unsuitable end-member for AFC models of the Underberg dyke suite, given its very high εNd value (+9). However, the most depleted rocks of the Underberg suite have εNd_i values of +1 and $^{87}Sr/^{86}Sr_i$ values of ∼0·7045, and provide a more feasible end-member for the remainder of the Underberg suite; this is akin to the composition of the Rooi Rand dykes.

Using both Namaqua–Natal Belt granitoid and the Ecca Group hornfels as potential crustal contaminants, AFC processes were modelled using an Underberg depleted composition as the magma end-member (Fig. 11). Employing the AFC model of De Paolo (1981),

Table 3: EC-AFC parameters

Thermal parameters		
Magma liquidus temperature	1210°C	
Magma initial temperature	1210°C	
Assimilant liquidus temperature	1100°C	
Assimilant initial temperature	660°C	
Solidus temperature	950°C	
Isobaric specific heat of magma (J/kg K)	1495	
Fusion enthalpy (J/kg)	354000	
Isobaric specific heat of assimilant (J/kg K)	1400	
Crystallization enthalpy of recharge magma	396000	
Isobaric specific heat of recharge magma (J/kg K)	1500	
Compositional parameters		
Element	Sr	Nd
Magma concentration	338	15
Bulk D_0	0·8	0·1
Enthalpy	0	0
Assimilant concentration	279	80
Bulk D_0	0·4	0·5
Enthalpy	0	0
Isotope	$^{87}Sr/^{86}Sr$	εNd
Ratio magma	0·7045	1
Ratio assimilant	0·71	−4

the Namaqua–Natal granitoid is an unsuitable contaminant composition (Fig. 11); however, the Ecca Group hornfels provides a more suitable contaminant composition to fit the Underberg dyke suite. Using the geologically reasonable parameters set out in Table 3, several of the Underberg dykes could reasonably be interpreted as the products of AFC involving a hornfels contaminant, although the levels of contamination using the De Paolo model are probably too high. Employing the EC-RAFC model of Spera & Bohrson (2004), and using the Ecca Group hornfels as a contaminant composition, generates an appropriate trend for the Underberg dyke suite with geologically reasonable contamination values. The EC-RAFC model was run with an initial magma liquidus temperature estimate of 1210°C and a temperature interval of ~7·5°C (full details are given in Table 4). The samples with the most negative εNd values (<−3) are not well represented given an equilibration temperature of ~1000°C. However, in general terms, an AFC model involving the most depleted Underberg composition and a local contaminant could generate some of the variation observed in the Underberg suite.

Lithospheric mantle enrichment

Mantle metasomatism is believed to be the key process responsible for the enrichment of the lithospheric mantle (e.g. Menzies & Hawkesworth, 1987). The lithospheric mantle beneath the Archaean craton of southern Africa has been extensively modally metasomatized, evidenced from a detailed study of peridotite xenoliths (Erlank *et al.*, 1987).

A key process, which has been suggested in the petrogenesis of many CFB provinces, is the contamination of 'primary' basaltic magmas with partial melts of enriched lithospheric mantle (e.g. Ellam & Cox, 1991; Luttinen & Furnes, 2000), with contamination taking place before the magmas reach crustal level. As discussed above, the trace element patterns of many of the Underberg dykes (and other Karoo rocks) are characterized by negative anomalies in the HFSE, typical of arc-related basalts. As there was no active continental margin at the time of Karoo magmatism, the arc-like signature must be a remnant of pre-existing subduction. To categorize the amount of subduction-derived fluid added to the mantle, as well as the degree of partial melting, it is helpful to examine incompatible trace element ratios, such as La/Yb and Ba/Nb (Guo *et al.*, 2005). In addition to being reliable indicators of partial melting and subduction fluid addition, the ratios La/Yb and Ba/Nb are not affected by small amounts of fractional crystallization of olivine and clinopyroxene. Guo *et al.* (2005) developed a mixing and partial melting model for these trace elements to simulate the petrogenesis of potassic magmas from SE Tibet. The model assumes that the magmas were generated in two stages: (1) mixing of depleted mantle and subduction-derived fluid; (2) partial melting of the resultant enriched mantle. The starting composition is taken as N-MORB source mantle, which has trace element abundances equivalent to 0·1 times N-MORB (Sun & McDonough, 1989), as MORB magmas are ~10% partial melts of N-MORB source mantle. The composition of the subduction-derived fluid is less straightforward, as the abundances of La, Yb, Ba and Nb vary significantly (e.g. Tatsumi & Hanyu, 2003); therefore Guo *et al.* (2005) used two different fluid compositions in their models, one with high abundances (Fluid A), the other with low abundances (Fluid B) (Fig. 12). The mixing model between depleted mantle and the two fluid compositions are shown in Fig. 12 for non-modal batch partial melting models and the Underberg dykes are plotted. The Underberg dykes have low values of both Ba/Nb and La/Yb and plot close to the origin of the mixing curves of Guo *et al.* (2005). The mixing model using the Fluid A composition (high concentrations of La, Yb, Nb, Ba) indicates that the Underberg dykes have a very low content of the subduction-derived fluid, typically <0·2% (Fig. 12a). The mixing model using the Fluid B composition (low concentrations of La, Yb, Nb, Ba) shows that the Underberg dykes also have a relatively small contribution from the subduction-derived fluid, typically <10% (Fig. 12b), although clearly much greater than the Fluid A model. The non-modal partial melting model indicates a degree of mantle partial melting of ~15%. The samples

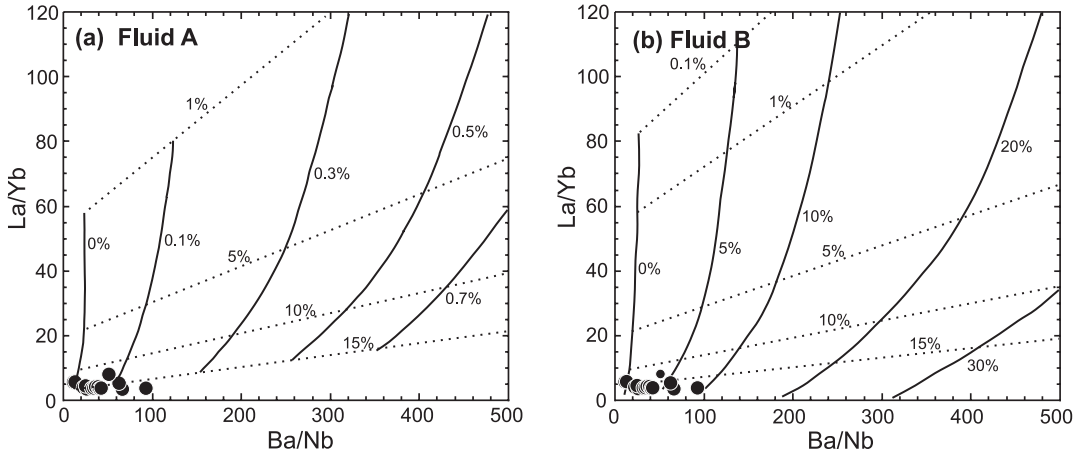

Fig. 12. Variation in La/Yb vs Ba/Nb. The numbers (%) along the dotted lines represent the degree of partial melting. The numbers (%) along the continuous lines (in italics) are the proportion of the subduction-derived fluid in the mantle source region. (a) Non-modal batch partial melting model calculated by Guo *et al.* (2004) for fluid composition A (Ba 2672 ppm, Nb 0 ppm, La 99 ppm, Yb 0·3 ppm) and (b) non-modal batch partial melting for fluid B (Ba 52 ppm, Nb 0 ppm, La 1·6 ppm, Yb 0 ppm).

that show the greatest contribution from a subduction-derived fluid are those with Ba/Nb values >60 and include the samples SA.3.1, SA.5.1 and SA.12.1, which also have amongst the highest $^{87}Sr/^{86}Sr_i$ values (0·7075–0·7100) and are 'Ferrar-like' in composition.

Links to Ferrar magmatism

Karoo and Ferrar tholeiites are considered geochemically distinct and geographically separate, with overlap known only in a few areas of pre-break-up Gondwana. Brewer *et al.* (1992) identified both Karoo- and Ferrar-like rocks in the Theron Mountains of Coats Land, Antarctica (Fig. 1), although they are chronologically distinct (193 Ma for Ferrar; 176 Ma for Karoo). Other workers have also speculated that Ferrar-like magmatic rocks might extend beyond the accepted limits of the Ferrar province (Fig. 1). Elliot & Fleming (2000) noted that the low-Ti, Golden Gate lavas of northern Lesotho (Fig. 1) are geochemically similar to the low-Ti tholeiites of the Ferrar province. The Golden Gate lavas have similar $^{87}Sr/^{86}Sr$ and εNd isotope ratios to the Ferrar intrusions (Fig. 11), which are distinctive when compared with other Karoo volcanic rocks. Elliot & Fleming (2000) concluded that the Golden Gate lavas were derived from the same source as the Ferrar, and suggested the interfingering of Ferrar-derived lavas with the lower units of the Karoo flood basalt sequence in Lesotho.

A geochemical study of the Mesozoic dolerite dykes of the Falkland Islands by Mitchell *et al.* (1999) also identified Karoo- and Ferrar-like rock types. An east–west-trending dyke group has compositional similarities (Fig. 11) to the Rooi Rand dyke swarm of the Karoo (Duncan *et al.*, 1990), whereas a north–south-trending dyke group is geochemically similar to Ferrar magmatic rocks (Fig. 11). Mitchell *et al.* (1999) also noted that rare samples of the north–south-trending suite are geochemically akin to the Kraai River volcanic rocks of southern Lesotho.

Several of the Underberg dykes (SA.3.1, SA.5.1, SA.6.1) have $^{87}Sr/^{86}Sr$ (0·7090–0·7100) and εNd (−3·8 to −14·5) values close to those of the Ferrar magmas (Fig. 11), although the sample with εNd = −14·5 is more akin to the low-εNd rocks of CT1 (Vestfjella; Luttinen & Furnes, 2000) and the basalts of the southern Lebombo (Sweeney *et al.*, 1994), and may reflect the incorporation of Precambrian LREE-enriched lithospheric material. The similarity to Ferrar rocks is also highlighted in Fig. 10, which shows that these three samples plot close to the Ferrar field and are distinct from the other Underberg dykes. A similar pattern is observed in Fig. 13, where Nb/Nb* is plotted against $^{87}Sr/^{86}Sr_i$. The Underberg dykes are plotted relative to a restricted (because of the absence of published Th data) range of Karoo and Ferrar rock types. The variation in Nb/Nb* relative to $^{87}Sr/^{86}Sr_i$ shows a trend towards lower Nb/Nb* values, indicating an increased contribution from the continental crust or melts from subduction-modified lithospheric mantle. The samples with the lowest Nb/Nb* and highest $^{87}Sr/^{86}Sr_i$ overlap with the field of Ferrar rock types.

The presence of Ferrar-like rocks in the Underberg region of southern KwaZulu-Natal, coupled with the 'Ferrar-like' Golden Gate lavas (Elliot & Fleming, 2000), suggests that there is a clear Ferrar component within the Karoo volcanic province. The composition of lava sequences from Moshesh's Ford and Kraai River, as well as several of the dykes from the Underberg suite, are intermediate between a Rooi Rand-like composition and a Ferrar-like composition, which prompts the suggestion that some of the variability could be explained by mixing of Ferrar and Karoo magma compositions.

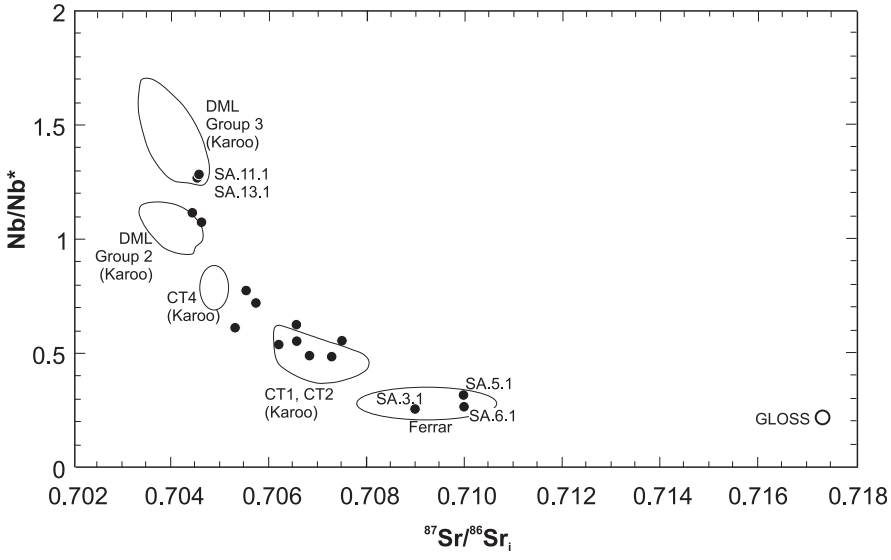

Fig. 13. Nb anomaly, Nb/Nb* [$= Nb_N\sqrt{(Th_N \times La_N)}$] vs $^{87}Sr/^{86}Sr$. The Nb anomaly can be used to test the role of sediment contamination in mantle-derived magmas. The DML Groups 2 and 3 field are from Riley *et al.* (2005). The CT1, 2, 4 fields are from the Karoo province in Vestfjella (Luttinen & Furnes, 2000). The Ferrar field is from Molzahn *et al.* (1996). GLOSS is average global subducting sediment (Plank & Langmuir, 1998); $^{87}Sr/^{86}Sr = 0{\cdot}7173$, Sr 327 ppm, Nb/Nb* = 0·22.

To test the possibility of Ferrar-sourced magmas being transported into the Karoo province, samples were selected for AMS analysis to determine the magma flow direction

MAGMA FLOW

Anisotropy of magnetic susceptibility (AMS) data

Background

Anisotropy of magnetic susceptibility (AMS) measurements have been shown to be a very sensitive technique for determining the flow direction of mafic magmas (e.g. Knight & Walker, 1988; Ernst & Baragar, 1992; Cañón-Tapia *et al.*, 1996; Liss *et al.*, 2002). With this aim, we collected oriented block samples from the margins of well-exposed dykes where the dyke–wall-rock contact was observed and surface weathering minimal. Of the dykes sampled for geochemistry only six possessed two exposed margins. Block samples were oriented in the field using a magnetic compass, and later drilled in the laboratory. The retrieved cores were measured on an AGICO KLY3 Kappabridge at the School of Geography, Earth and Environmental Sciences (University of Birmingham) to determine the three principal axes of magnetic susceptibility k_{max}, k_{int}, k_{min}. These principal axes define an ellipsoid of magnetic susceptibility, the shape of which is described by the magnetic lineation [$L = (k_{max} - k_{min})/k_{mean}$] and foliation [$F = (k_{int} - k_{min})/k_{mean}$]. The shape of the ellipsoid is indicated by the angle $\mu = \tan^{-1} L/F$ (the angle from the F axis to a point on a plot of L vs F, ranging from 0° for purely oblate to 90° for purely prolate), whereas the strength of the anisotropy is indicated by the total anisotropy ($H = L + F$). AMS data together with dyke orientation and width data are presented in Table 4.

AMS fabrics

The AMS fabrics predominantly fall into two distinct types, as follows.

(1) Type A fabrics are characterized by k_{min} axes clustering approximately normal to the dyke wall, and k_{max} and k_{int} forming a magnetic foliation sub-parallel to the intrusion plane (e.g. Fig. 14, sample SA.1.3). Such 'normal' AMS fabrics are interpreted to be the product of magma flow, with k_{max} parallel to flow (e.g. Knight & Walker, 1988; Ernst & Baragar, 1992; Rochette *et al.*, 1992). Normal magnetic fabrics account for 55% of the AMS fabrics measured in this study.

Type B fabrics are characterized by a cluster of k_{int} axes plotting approximately normal to the intrusion plane (e.g. Fig. 14, sample SA.14.3). Such 'intermediate fabrics' (Rochette *et al.*, 1999) have been variously related to the mixing of differing magnetite grain sizes (Rochette *et al.*, 1992), magmatic shear and associated rotation of ellipsoidal magnetite grains (Dragoni *et al.*, 1997), or the vertical compaction of a static magma column (Park *et al.*, 1988).

In addition to the normal and intermediate fabrics, two samples (SA.8.2 and SA.8.3) display abnormal AMS fabrics that are characterized by strongly prolate or oblate fabrics, where only one principal axis shows a good clustering of data, with the other two axes being widely

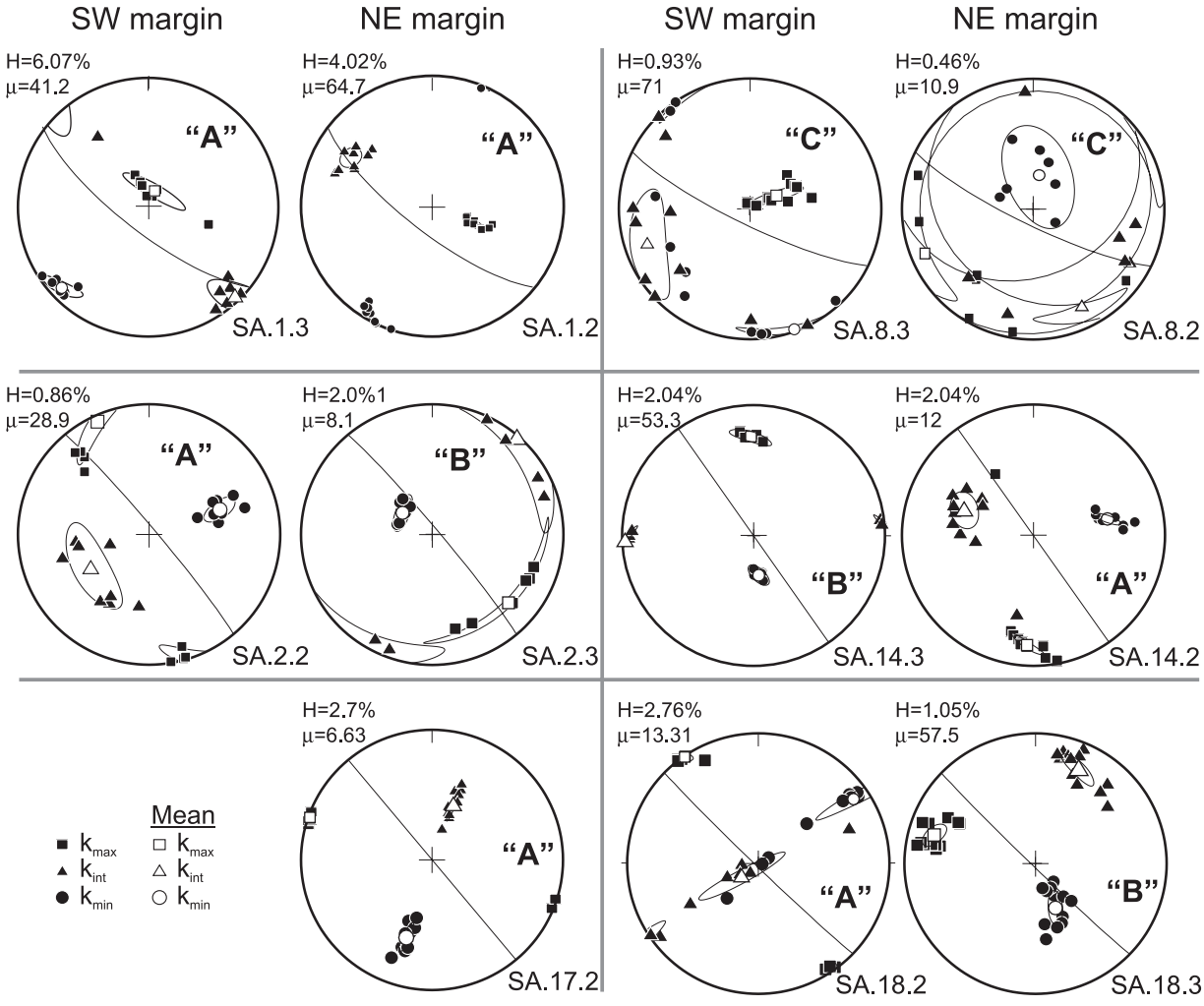

Fig. 14. Anisotropy of magnetic susceptibility results from six dykes within the KwaZulu-Natal dyke suite, with mean susceptibility axes (open symbols) and 95% confidence ellipses. Great circles represent dyke orientation.

distributed. These fabrics are denoted type C in Fig. 14 (samples SA.8.2 and SA.8.3).

Discussion and interpretation of AMS fabrics within the Underberg dyke suite

Interpretation of magma flow direction from the AMS fabrics obtained from the Underberg dykes is complicated by the presence of both normal and intermediate magnetic fabrics within the same dyke. However, a similar distribution of normal and intermediate fabrics was encountered in dykes within the Koolau complex, Hawaii (Knight & Walker, 1988), where both normal and intermediate fabrics displayed similarly oriented k_{max} axes, the orientations of which were sub-parallel to observed macroscopic magma flow indicators along the dyke margins. Knight & Walker (1988) concluded that the orientation of k_{max} in most of the dykes approximated the magma flow direction. This combination of AMS and field data indicates that intermediate fabrics can represent a simple switch between the k_{int} and k_{min} axes, whereas k_{max} (the magnetic lineation) remains parallel to magma flow, as predicted by numerical modelling of sheared ellipsoidal grains (Dragoni *et al.*, 1997) or some models for the proportional mixing of single-domain and multi-domain magnetite grains (Rochette *et al.*, 1992).

Knight & Walker (1988) also identified the presence of an obliquity of the magnetic lineation in each margin of a dyke (imbricate fabric) that was symmetrical about the centre of the intrusion plane and indicated the absolute magma flow direction. Other workers have successfully employed symmetrical imbricate AMS fabrics to determine an absolute flow direction in dykes, e.g. symmetric magnetic lineations (Tauxe *et al.*, 1998; Callot *et al.*, 2001) and symmetric magnetic foliation and lineation (Herrero-Bervera *et al.*, 2001).

Table 4: Summary of AMS data

Sample	*n*	K_m	*L*	*F*	*H*	μ	k_{max}	k_{int}	k_{min}	Strike/dip	Width (m)
SA.1.2	9	14647	2·73	1·29	4·02	64·7	111/62	301/29	209/04	218/75	15
SA.1.3	7	23793	2·83	3·23	6·07	41·2	021/80	136/04	226/09	218/75	15
SA.2.2	8	14622	0·3	0·55	0·86	28·9	335/05	239/47	070/42	050/86	4
SA.2.3	6	14037	0·25	1·76	2·01	8·1	132/23	041/02	306/67	050/86	4
SA.8.2	7	1433	0·07	0·38	0·46	10·9	247/11	153/17	010/68	206/80	3·5
SA.8.3	10	8283	0·69	0·24	0·93	71	063/71	250/18	160/02	206/80	3·5
SA.14.2	10	12726	0·36	1·68	2·04	12	183/16	289/43	77/41	055/90	10
SA.14.3	5	10578	1·17	0·87	2·04	53·3	358/25	267/02	172/64	055/90	10
SA.17.2	10	8666	2·35	0·35	2·70	6·63	289/01	021/52	198/37	050/90	10
SA.18.2	9	20107	2·56	0·19	2·76	13·31	325/01	231/76	055/13	224/88	10
SA.18.3	12	21475	0·64	0·41	1·05	57·5	285/20	024/21	156/59	224/88	10

n, number of samples measured, K_m, mean susceptibility, $L = (k_{max} - k_{min})/k_{mean}$; $F = (k_{int} - k_{min})/k_{mean}$; $H = (L + F)$; *m*, magnetic fabric shape (oblate, 0–25; triaxial, 25–65; prolate, 65–90).

In the case of the Underberg dyke suite, we consider that five of the six dykes analysed provide evidence for magma flow direction, with two indicating absolute (known direction) magma flow directions. Figure 15a and b presents paired AMS fabrics from opposite margins of two dykes (SA.2 and SA.18) where both dykes show normal and intermediate fabrics in opposite margins. We have dismissed vertical compaction of a static magma column as a cause for the intermediate fabrics, as we would expect intermediate fabrics to have formed at both margins. As the k_{max} axes for both normal and intermediate fabrics are sub-parallel, we have assumed that the intermediate fabrics represent a switching of k_{min} and k_{int}, as a result of either magma-related shear (Dragoni *et al.*, 1997) or the mixing of single-domain and multi-domain magnetite grains (Rochette *et al.*, 1992, fig. 8b). In both dykes, the magnetic lineations (k_{max}) are oblique to their respective margins and are symmetrical about the centre line of the dyke. Along the southwestern margins of the dykes k_{max} lies clockwise oblique to the dyke wall, whereas a counter-clockwise obliquity is found along the NE margins. In addition, the magnetic foliation of normal AMS fabrics also forms a clockwise imbrication angle with respect to the southwestern dyke margin. This symmetrical geometry combined with sub-horizontal k_{max} suggests that magma flowed laterally from the SE to NW.

Dyke SA.17, for which only one sample from the NE margin returned useable cores, possesses a highly prolate fabric ($\mu = 82$) with a horizontal k_{max} lying counter-clockwise oblique to the dyke margin (Fig. 15c). This sense of imbrication is consistent with that observed in NE margins of dykes SA.2 and SA.18, and in the absence of contrary data from the SW dyke margin, we interpret the AMS fabric of SA.17 also to be the result of lateral magma flow from the SE to NW.

Dyke SA.14 again displays both normal and intermediate fabrics. Along its NE margin a strongly oblate ($\mu = 12$) normal fabric was measured that possesses a sub-horizontal k_{max}, whereas a triaxial ($\mu = 53$) intermediate fabric with sub-horizontal k_{max} was measured along the SE margin (Fig. 15d). Despite both AMS fabrics displaying consistent shallowly plunging k_{max} axes, unlike dykes SA.2 and SA.18 there is no symmetry of the magnetic lineation across the dyke, and thus the AMS results are difficult to interpret in terms of absolute magma flow direction. However, the fabrics are potentially explained by the theoretical model of Dragoni *et al.* (1997), which, as well as predicting the periodic switch of k_{int} and k_{min} to form intermediate fabrics, suggests that the magnetic lineation (k_{max}) oscillates in a plane parallel to the flow direction and perpendicular to the intrusion plane (±45°) as a function of strain (magma flow). Thus the fabrics recognized in SA.14 are theoretically possible. Perhaps the most significant aspect of the Dragoni *et al.* (1997) model in this instance is that k_{max} remains parallel to the magma flow direction, even when intermediate fabrics form; therefore, the AMS fabrics from SA.14 may be indicative of lateral magma flow, although the absolute direction cannot be determined. An interpretation of lateral magma flow is consistent with the presence of scarce sub-horizontally stretched amygdales within the dyke.

Dyke SA.1 possesses normal magnetic fabrics at both margins (Fig. 15e), characterized by steeply dipping magnetic foliations, sub-parallel to the strike of the intrusion plane and sub-vertical k_{max}. However, the obliquity of the magnetic foliation is not symmetrical about the

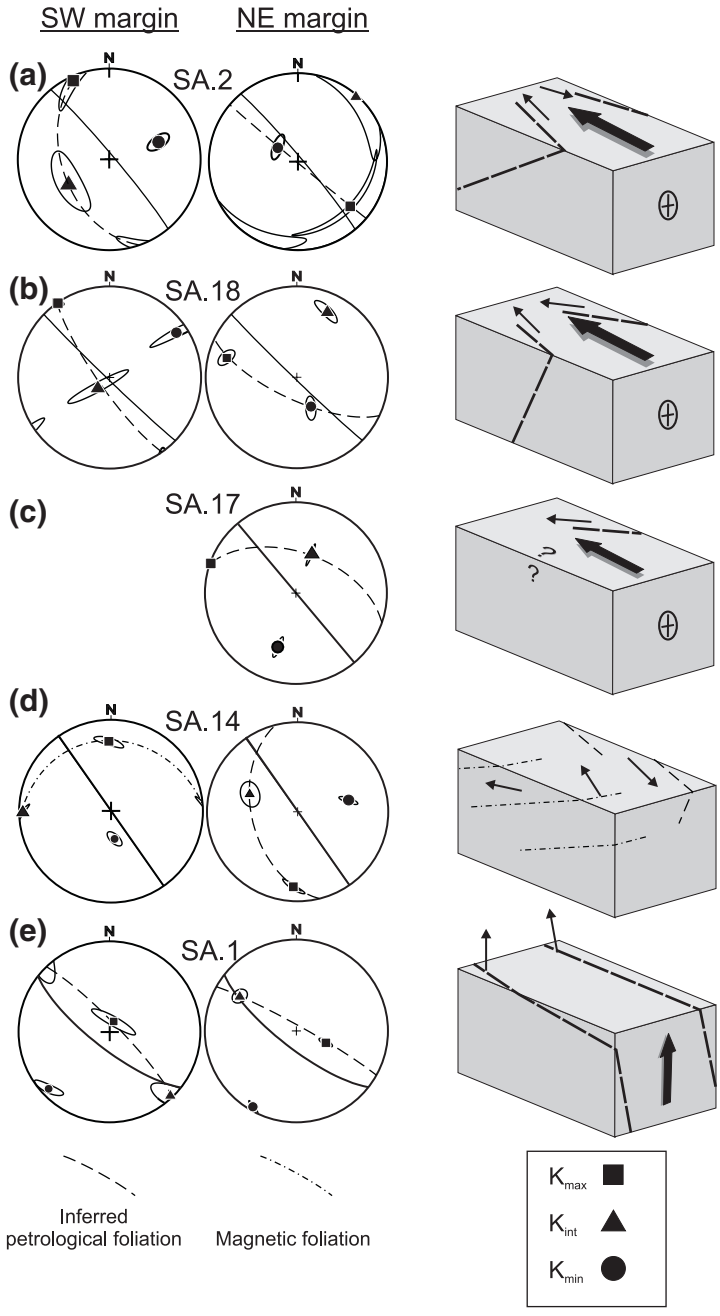

Fig. 15. (a–e) Equal area stereograms displaying the mean susceptibility axes k_{max}, k_{int}, k_{min}, plus 95% confidence ellipses for samples from the KwaZulu-Natal dyke suite. Intermediate fabrics are interpreted to be the product of a switching of k_{int} and k_{min} axes, thus the inferred petrological foliation is interpreted as containing k_{max} and k_{min}. Block diagrams in (a–e) summarize the relationship of the inferred imbricate petrological foliation and lineation to dyke margins. Inferred petrological lineation is considered parallel to k_{max}, and with the petrological foliation is equivalent to the magnetic foliation in normal fabrics and the plane containing k_{max} and k_{min} in intermediate fabrics (see discussion in text).

dyke centre, thus absolute magma flow determination is not possible. The presence of normal fabrics with sub-vertical k_{max} axes strongly suggests vertical magma flow.

Samples from dyke SA.8 possess a low total anisotropy (H = 0·93–0·46) and show a correspondingly wider spread of data (Fig. 14). The AMS fabrics are also diverse. The SW margin displays a prolate fabric with k_{max} being sub-vertical and lying close to the intrusion plane, with k_{int} and k_{min} forming an overlapping distribution perpendicular to k_{max}. The NE margin reveals an oblate fabric with k_{min} occupying a sub-vertical position within the intrusion plane, and k_{max} and k_{int} forming a scattered distribution perpendicular to k_{min}.

The presence of diverse AMS fabrics within the sampled dykes of the Underberg dyke suite complicates interpretations of relative and/or absolute magma flow. However, we have interpreted the intermediate AMS fabrics potentially to be a product of mixed components of multi-domain and single-domain magnetite, or shearing of elliptical magnetite grains by flowing magma, with both explanations allowing the switching of k_{min} and k_{int}, whereas k_{max} remains parallel to the magma flow direction. Using this interpretation we conclude that four of the six dykes analysed show evidence for lateral magma flow, with three dykes suggesting absolute magma flow from the SE to NW, whereas one dyke shows evidence of subvertical magma flow.

SUMMARY

Geochemical evidence from this study, and that of Elliot & Fleming (2000), indicates the extension of Ferrar-like intrusions and lavas into the Karoo volcanic province. The Golden Gate lavas of northern Lesotho and at least three of the Underberg dykes have isotopic and trace element characteristics typical of Ferrar lavas and intrusions (e.g. Hergt, 2000). Several other dykes from the KwaZulu-Natal have geochemical characteristics that suggest they may contain a Ferrar component (Fig. 11).

The occurrence of Ferrar-sourced intrusive rocks has also been reported from the Falkland Islands (Mitchell *et al.*, 1999) and the Theron Mountains (Brewer *et al.*, 1992), where they occur in close association with Karoo-like igneous rocks. The geographical locations of these areas, combined with the Underberg dykes of southern KwaZulu-Natal and the Lesotho Highlands, would all have been in close proximity in Gondwana reconstructions (Fig. 1).

The AMS fabrics of the Underberg dykes are diverse and interpretations are not straightforward. Interpretation of intermediate fabrics combined with normal fabrics suggests that four of the six analysed dykes show evidence for lateral flow, and three dykes indicate that flow was directed from the SE toward the NW. This direction is consistent in Gondwana reconstructions with lateral magma flow from the Ferrar source region (Fig. 1). However, stratigraphical studies (Haycock *et al.*, 1997) suggest that the dykes must have been emplaced at shallow levels, a consideration that does not prohibit lateral magma flow, as examples of lateral magma flow in shallow (<4 km) dykes have been described (Callot *et al.*, 2001), but does question how far magma can flow laterally from its source at such shallow depths. The presence of dykes displaying evidence for subvertical magma flow might suggest that that the Underberg dyke suite may be related to a closer magma source/s, with the magma flow trajectory forming a fan-like pattern with sub-horizontal flow further away from the source, and the trajectory steepening and converging towards the source in a similar manner to the inferred magma flow trajectories for the Rio Ceará–Mirim dykes of NE Brazil (Archanjo *et al.*, 2000). Unfortunately, our study did not allow for an along-strike analysis of magma flow trajectories within the Underberg dykes, which would be necessary to determine if the evidence for horizontal flow is regional or related to more local magma centres to the SE.

CONCLUSIONS

(1) The mafic dykes near Underberg (southern KwaZulu-Natal) trend approximately NW–SE and extend SE from the Karoo central area of Lesotho toward the coast. The dyke suite was intruded at ~178 Ma (176·4 ± 1·2 to 181·7 ± 0·7 Ma) and is coincident in age with the major Okavango dyke swarm of southern Botswana.

(2) The dykes are all low-TiO_2–Zr tholeiites with TiO_2 <1·5 wt %, Zr <150 ppm and Ti/Y <310, but display a broad Nd–Sr isotopic range; they vary from 'depleted' Rooi Rand-like compositions ($^{87}Sr/^{86}Sr$ ~0·7045, εNd ~1) to 'enriched' Ferrar-like compositions ($^{87}Sr/^{86}Sr$ ~0·710, εNd ~ −9).

(3) Analysis of AFC (and EC-RAFC) models indicates that some of the variation seen in the Underberg dyke suite and also the lava units of Moshesh's Ford and Kraai River could be the result of combined assimilation and fractional crystallization from a Rooi Rand-like parent magma and a local upper crust contaminant (Ecca Group hornfels). However, those samples with more negative εNd and more radiogenic $^{87}Sr/^{86}Sr$ (i.e. more 'Ferrar-like') are not well represented using AFC models.

(4) To assess the role of lithospheric mantle enrichment in the petrogenesis of the Underberg dykes, we have used the element ratios Ba/Nb and La/Yb. Two models are examined here, which use two different fluid compositions; one with high concentrations and the other with low. Even using a model subduction-derived fluid with low concentrations of Ba, Nb, La and Yb, it is clear that the Underberg dykes are not derived from a lithospheric mantle source strongly enriched by a subduction-derived component. The three samples with 'Ferrar-like' geochemical characteristics tend to have the highest Ba/Nb values and are, therefore, derived from a source with at least some degree of enrichment, presumably derived from subduction-derived fluids.

(5) At least three of the Underberg dykes are derived from a magma source akin to the source that generated the Ferrar magmatic province. Several of the other dykes, as well as lavas from Kraai River and Moshesh's Ford, are possible Karoo–Ferrar hybrid compositions.

(6) AMS data suggest that four of the six dykes analysed show evidence for lateral magma flow, with three dykes

(SA.2, SA.17, SA.18) suggesting an absolute flow direction from the SE to the NW. The three samples lie on, or close to, a putative mixing curve between a Ferrar end-member and a depleted mantle end-member. An absolute flow direction from the SE is in agreement with the geochemistry, which supports a Ferrar magma component in the Underberg dyke suite. However, we cannot determine if lateral magma transport occurred at a regional scale from a distant magma source, or on a more localized scale.

ACKNOWLEDGEMENTS

This manuscript has benefited considerably from the thoughtful and thorough reviews of Chris Harris, Janet Hergt, Goonie Marsh and Marjorie Wilson. Graham Pearson (University of Durham) supplied the ICP-MS analyses, Dave Emley (University of Keele) carried out the XRF analyses, and John Huard (Oregon State University) assisted with the $^{40}Ar/^{39}Ar$ geochronology.

REFERENCES

Allsopp, H. L., Bristow, J. W., Logan, C. T., Eales, H. V. & Erlank, A. J. (1984). Rb–Sr geochronology of three Karoo-related intrusive complexes. In: Erlank, A. J. (ed.) *Petrogenesis of the Volcanic Rocks of the Karoo Province. Geological Society of South Africa, Special Publication* **13**, 281–287.

Antonini, P., Picciirillo, E. M., Petrini, R., Civetta, L., D'Antonio, M. & Orsi, G. (1999). Enriched mantle–Dupal signature in the genesis of the Jurassic Ferrar tholeiites from Prince Albert Mountains (Victoria Land, Antarctica). *Contributions to Mineralogy and Petrology* **136**, 1–19.

Archanjo, C. J., Trindade, R. I., Macedo, J. W. P. & Araújo, M. G. (2000). Magnetic fabric of a basaltic dyke swarm associated with Mesozoic rifting in northeastern Brazil. *Journal of South American Earth Sciences* **13**, 179–189.

Brewer, T. S., Hergt, J. M., Hawkesworth, C. J., Rex, D. & Storey, B. C. (1992). Coats Land dolerites and the generation of Antarctic continental flood basalts. In: Storey, B., Alabaster, T. & Pankhurst, R. (eds) *Magmatism and the Causes of Continental Break-up. Geological Society, London, Special Publications* **68**, 185–208.

Callot, J.-P., Geoffroy, L., Aubourg, C., Pozzi, J. P. & Mege, D. (2001). Magma flow directions of shallow dykes from the East Greenland volcanic margin inferred from magnetic fabric studies. *Tectonophysics* **335**, 313–329.

Cañón-Tapia, E., Walker, G. P. L. & Herrero-Bervera, E. (1996). The internal structure of lava flows—insights from AMS measurements 1: Near vent a'a. *Journal of Volcanology and Geothermal Research* **70**, 21–36.

Chevallier, L. & Woodford, A. (1999). Morpho-tectonics and mechanism of emplacement of the dolerite rings and sills of the western Karoo, South Africa. *South African Journal of Geology* **102**, 43–54.

Cox, K. G. (1988). Numerical modelling of a randomized RTF magma chamber: a comparison with continental flood basalt sequences. *Journal of Petrology* **29**, 681–698.

Cox, K. G. (1992). Karoo igneous activity, and the early stages of the break-up of Gondwanaland. In: Storey, B. C., Alabaster, T. & Pankhurst, R. J. (eds) *Magmatism and the Causes of Continental Break-up. Geological Society, London, Special Publications* **68**, 137–148.

Cox, K. G., MacDonald, R. & Hornung, G. (1967). Geochemical and petrographic provinces in the Karoo basalts of southern Africa. *American Mineralogist* **52**, 1451–1474.

DePaolo, D. J. (1981). Trace element and isotopic effects of combined wallrock assimilation and fractional crystallization. *Earth and Planetary Science Letters* **53**, 189–202.

Dragoni, M., Lanza, R. & Tallarico, A. (1997). Magnetic anisotropy produced by magma flow: theoretical model and experiemtal data from Ferrar dolerite sills (Antarctica). *Geophysical Journal International* **128**, 230–240.

Duncan, A. R., Armstrong, R. A., Erlank, A. J., Marsh, J. S. & Watkins, R. T. (1990). MORB-related dolerites associated with the final phases of Karoo flood basalt volcanism in southern Africa. In: Parker, A. J., Rickwood, P. C. & Tucker, D. H. (eds) *Mafic Dykes and Emplacement Mechanisms*. Rotterdam: Balkema, pp. 119–129.

Duncan, R. A., Hooper, P. R., Rehacek, J., Marsh, J. S. & Duncan, A. R. (1997). The timing and duration of the Karoo igneous event, southern Gondwana. *Journal of Geophysical Research* **102**, 18127–18138.

Eglington, B. M. & Armstrong, R. A. (2003). Geochronological and isotopic constraints on the Mesoproterozoic Namaqua–Natal Belt: evidence from deep borehole intersections in South Africa. *Precambrian Research* **125**, 179–189.

Elburg, M. & Goldberg, A. (2000). Age and geochemistry of Karoo dolerite dykes form northeast Botswana. *Journal of African Earth Sciences* **31**, 539–554.

Ellam, R. M. & Cox, K. G. (1991). An interpretation of Karoo picrite basalts in terms of interaction between asthenospheric magmas and the mantle lithosphere. *Earth and Planetary Science Letters* **105**, 330–342.

Ellam, R. M., Carlson, R. W. & Shirley, S. B. (1992). Evidence from Re–Os isotopes for plume–lithosphere mixing in Karoo flood basalt genesis. *Nature* **359**, 718–721.

Elliot, D. H. & Fleming, T. H. (2000). Weddell triple junction: the principal focus of Ferrar and Karoo magmatism during initial breakup of Gondwana. *Geology* **28**, 539–542.

Elliot, D. H., Fleck, R. J. & Sutter, J. F. (1985). K-Ar age determinations of Ferrar Group rocks, central Trnsantarctic Mountains. *Antarctic Research Series* **36**, 197–224.

Elliot, D. H., Fleming, T. H., Kyle, P. R. & Foland, K. A. (1999). Long-distance transport of magmas in the Jurassic Ferrar large igneous province, Antarctica. *Earth and Planetary Science Letters* **167**, 89–104.

Encarnación, J., Fleming, T. H., Elliot, D. H. & Eales, H. V. (1996). Synchronous emplacement of Ferrar and Karoo dolerites and the early breakup of Gondwana. *Geology* **24**, 535–538.

Erlank, A. J. (1984). *Petrogenesis of the Volcanic Rocks of the Karoo Province. Geological Society of South Africa, Special Publication* **13**.

Erlank, A. J., Waters, F. G., Hawkesworth, C. J., Haggerty, S. E., Allsopp, H. L., Rickard, R. S. & Menzies, M. A. (1987). Evidence for mantle metasomatism in peridotite nodules from the Kimberley pipes, South Africa. In: Menzies, M. A. & Hawkesworth, C. J. (eds) *Mantle Metasomatism*. London: Academic Press, pp. 221–311.

Ernst, R. E. & Baragar, W. R. A. (1992). Evidence from magnetic fabric from the flow pattern of the magma in the Mackenzie giant radiating dyke swarm. *Nature* **356**, 511–513.

Faure, G., Bowman, J. R., Elliot, D. H. & Jones, L. M. (1974). Strontium isotope composition and petrogenesis of the Kirkpatrick Basalt, Queen Alexandra Range, Antarctica. *Contributions to Mineralogy and Petrology* **48**, 153–169.

Faure, G., Pace, K. K. & Elliot, D. H. (1982). Systematic variations in $^{87}Sr/^{86}Sr$ ratios and major element concentrations in the Kirkpatrick Basalt of Mount Falla, Queen Alexandra Range, Transantarctic Mountains. In: Craddock, C. (ed.) *Antarctic Geosciences*. Madison, WI: University of Wisconsin Press, pp. 15–723.

Fitch, F. J. & Miller, J. A. (1984). Dating of Karoo igneous rocks by the conventional K–Ar and $^{40}Ar/^{39}Ar$ age spectrum methods. In: Erlank, A. J. (ed.) *Petrogenesis of the Volcanic Rocks of the Karoo Province. Geological Society of South Africa, Special Publication* **13**, 247–266.

Fleming, T. H., Heimann, A., Foland, K. A. & Elliot, D. H. (1997). $^{40}Ar/^{39}Ar$ geochronology of Ferrar dolerite sills from the Transantarctic Mountains, Antarctica: implications for the age and origin of the Ferrar magmatic province. *Geological Society of America Bulletin* **109**, 533–546.

Floyd, P. A. (1985). Petrology and geochemistry of intraplate sheet-flow basalts, Nauru Basin, Deep Sea Drilling Project leg 89. In: Moberley, R. & Schlanger, S. O. (eds) *Initial Reports of the Deep Sea Drilling Project, 89*. Washington, DC: US Government Printing Office, pp. 471–497.

Fowler, S. J., Bohrson, W. A. & Spera, F. J. (2004). Magmatic evolution of the Skye igneous centre, western Scotland: modelling of assimilation, recharge and fractional crystallization. *Journal of Petrology* **45**, 2481–2505.

Guo, Z., Hertogen, J., Liu, J., Pasteels, P., Boven, A., Punzalan, L., He, H., Luo, X. & Zhang, W. (2005). Potassic magmatism in western Sichuan and Yunnan Provinces, SE Tibet, China: petrological and geochemical constraints on petrogenesis. *Journal of Petrology* **46**, 33–78.

Harmer, R. E., Lee, C. A. & Eglington, B. M. (1998). A deep mantle source for carbonatite magmatism: evidence from the nephelinites and carbonatites of the Buhera district, SE Zimbabwe. *Earth and Planetary Science Letters* **158**, 131–142.

Harris, C., Marsh, J. S., Duncan, A. R. & Erlank, A. J. (1990). The petrogenesis of the Kirwan Basalts of Dronning Maud Land, Antarctica. *Journal of Petrology* **31**, 341–369.

Hawkesworth, C. J., Marsh, J. S., Duncan, A. R., Erlank, A. J. & Norry, M. J. (1984). The role of continental lithosphere in the generation of the Karoo volcanic rocks: evidence from combined Nd- and Sr-isotope studies. In: Erlank, A. J. (ed.) *Petrogenesis of the Volcanic Rocks of the Karoo Province. Geological Society of South Africa, Special Publication* **13**, 341–354.

Hawkesworth, C. J., Kelley, S. P., Turner, S. P., le Roex, A. P. & Storey, B. C. (1999). Mantle processes during Gondwana break-up. *Journal of South African Earth Sciences* **28**, 239–261.

Haycock, C. A., Mason, T. R. & Watkeys, M. K. (1997). Early Triassic palaeoenvironments in the eastern Karoo foreland basin, South Africa. *Journal of South African Earth Sciences* **24**, 79–94.

Heimann, A., Fleming, T. H., Elliot, D. H. & Foland, K. A. (1994). A short interval of Jurassic continental flood basalt volcanism in Antarctica as demonstrated by $^{40}Ar/^{39}Ar$ geochronology. *Earth and Planetary Science Letters* **121**, 19–41.

Hergt, J. M. (2000). Comment on: 'Enriched mantle–Dupal signature in the genesis of the Jurassic Ferrar tholeiites from Prince Albert Mountains (Victoria Land, Antarctica)' by Antonini *et al.* (*Contributions to Mineralogy and Petrology* **136**, 1–19). *Contributions to Mineralogy Petrology* **139**, 240–244.

Hergt, J. M., Peate, D. W. & Hawkesworth, C. J. (1991). The petrogenesis of Mesozoic Gondwana low-Ti flood basalts. *Earth and Planetary Science Letters* **105**, 134–148.

Herrero-Bervera, E., Walker, G. P. L., Cañón -Tapia, E. & Garcia, M. O. (2001). Magnetic fabric and inferred flow direction of dikes, conesheets and sill swarms, Isle of Skye, Scotland. *Journal of Volcanology and Geothermal Research* **106**, 195–210.

Jones, D. L., Duncan, R. A., Briden, J. C., Randall, D. E. & MacNiocaill, C. (2001). Age of the Bakota basalts, northern Zimbabwe, and the duration of Karoo large igneous province magmatism. *Geochemistry, Geophysics, Geosystems* **2**, 2000GC000110.

Knight, M. D. & Walker, G. P. L. (1988). Magma flow directions in dykes of the Koolau Complex, Oahu, determined from magnetic fabric studies. *Journal of Geophysical Research* **93**, 4301–4319.

Koppers, A. A. P. (2002). ArArCALC—software for Ar-40/Ar-39 age calculations. *Computers and Geosciences* **28**, 605–619.

Kyle, P. R. (1980). Development of heterogeneities in the subcontinental mantle: evidence from the Ferrar Group, Antarctica. *Contributions to Mineralogy and Petrology* **73**, 89–104.

Le Bas, M. J., Le Maitre, R. W., Streckeisen, A. & Zanettin, B. (1986). A chemical classification of volcanic rocks based on the total alkali–silica diagram. *Journal of Petrology* **27**, 745–750.

Le Gall, B., Tshoso, G., Jourdan, F., Féraud, G., Bertrand, H., Tiercelin, J. J., Kampunzu, A. B., Modisi, M. P., Dyment, J. & Maia, M. (2002). $^{40}Ar/^{39}Ar$ geochronology and structural data from the giant Okavango and related mafic dyke swarms, Karoo igneous province, northern Botswana. *Earth and Planetary Science Letters* **202**, 595–606.

Lightfoot, P. C. & Naldrett, A. J. (1984). Chemical variation in the Insizwa Complex, Transkei, and the nature of the parent magma. *Canadian Mineralogist* **22**, 169–187.

Liss, D., Hutton, D. H. W. & Owens, W. H. (2002). Ropy flow structures: a neglected indicator magma-flow direction in sills and dykes. *Geology* **30**, 715–718.

Luttinen, A. V. & Furnes, H. (2000). Flood basalts of Vestfjella: Jurassic magmatism across an Archaean–Proterozoic lithospheric boundary in Dronning Maud Land, Antarctica. *Journal of Petrology* **41**, 1271–1305.

Marsh, J. S., Hooper, P. R., Rehacek, J., Duncan, R. A. & Duncan, A. R. (1997). Stratigraphy and age of Karoo basalts of Lesotho and implications for correlations with the Karoo igneous province. In: Mahoney, J. J. & Coffin, M. F. (eds) *Large Igneous Provinces: Continental, Oceanic, and Planetary Flood Volcanism. Geophysical Monograph, American Geophysical Union* **100**, 247–272.

Menzies, M. A. & Hawkesworth, C. J. (eds) (1987). *Mantle Metasomatism*. London: Academic Press.

Minor, D. R. & Mukasa, S. B. (1997). Zircon U–Pb and hornblende $^{40}Ar–^{39}Ar$ ages for the Dufek layered mafic intrusion, Antarctica: implications for the age of the Ferrar large igneous province. *Geochimica et Cosmochimica Acta* **61**, 2497–2504.

Mitchell, C., Ellam, R. M. & Cox, K. G. (1999). Mesozoic dolerite dykes of the Falkland Islands: petrology, petrogenesis and implications for geochemical proivinciality in Gondwanaland low-Ti basaltic rocks. *Journal of the Geological Society, London* **156**, 901–916.

Molzahn, M., Reisberg, L. & Wörner, G. (1996). Os, Sr, Nd, Pb and O isotope and trace element data from the Ferrar flood basalts, Antarctica: evidence for an enriched subcontinental lithospheric source. *Earth and Planetary Science Letters* **144**, 529–546.

Nakamura, N. (1974). Determination of REE, Ba, Fe, Mg, Na and K in carbonaceous and ordinary chondrites. *Geochimica et Cosmochimica Acta* **38**, 757–773.

Ottley, C. J., Pearson, D. G. & Irvine, G. J. (2003). A routine method for the dissolution of geological samples for the analysis of REE and trace elements via ICP-MS. In: Warwick, p. (ed.), *Plasma Source Mass Spectrometry*. Environmental Radiochemical Analysis II, *Special Publication 291, Royal Society of Chemistry* 221–230.

Pálfy, J. & Smith, P. L. (2000). Synchrony between Early Jurassic extinction, oceanic anoxic event, and the Karoo–Ferrar flood basalt volcanism. *Geology* **28**, 747–750.

Pankhurst, R. J. & Rapela, C. R. (1995). Production of Jurassic rhyolites by anatexis of the lower crust of Patagonia. *Earth and Planetary Science Letters* **134**, 23–36.

Park. K., Tanczyk, E. I. & Desbarats, A. (1988). Magnetic fabric and its significance in the 1400 Ma Mealy diabase dykes of Labrador, Canada. *Journal of Geophysical Research* **93**, 13689–13704.

Pearce, J. A. & Peate, D. W. (1995). Tectonic implications of the composition of volcanic arc magmas. *Annual Review of Earth and Planetary Sciences* **23**, 251–285.

Peate, D.W. (1997). The Paraná–Etendeka Province. In: Mahoney, J. J. & M. Coffin, M. F. (eds) *Large Igneous Provinces: Continental, Oceanic, and Planetary Flood Volcanism. Geophysical Monograph, American Geophysical Union* **100**, 217–245.

Plank, T. & Langmuir, C. H. (1998). The chemical composition of subducting sediment and its consequences for the crust and mantle. *Chemical Geology* **145**, 325–394.

Puffer, J. H. (2001). Contrasting high field strength element contents of continental flood basalts from plume vs reactivated-arc sources. *Geology* **29**, 675–678.

Renne, P. R., Deino, A. L., Walter, R. C., Turrin, B. D., Swisher, C. C., Becker, T. A., Curtis, G. H., Sharp, W. D. & Jaouni, A.-R. (1994). Intercalibration of astronomical and radioisotopic time. *Geology* **22**, 783–786.

Renne, P. R., Swisher, C. C., Deino, A. L., Karner, D. B., Owens, T. L. & DePaolo, D. J. (1998). Intercalibration of standards, absolute ages 1and uncertainties in Ar–Ar dating. *Chemical Geology* **145**, 117–152.

Riley, T. R. & Knight, K. B. (2001). Age of pre-break-up Gondwana magmatism: a review. *Antarctic Science* **13**, 99–110.

Riley, T. R., Millar, I. L., Watkeys, M. K., Curtis, M. L., Leat, P. T., Klausen, M. B. & Fanning C. M. (2004). U–Pb zircon (SHRIMP) ages for the Lebombo rhyolites, South Africa: refining the duration of Karoo volcanism. *Journal of the Geological Society, London* **161**, 542–545.

Riley, T. R., Leat, P. T., Curtis, M. L., Millar, L. L. & Fazel, A. (2005). Early–Middle Jurassic dolerite dykes from western Dronning Maud Land (Antarctica): identifying mantle sources in the Karoo large igneous province. *Journal of Petrology* **46**, 1489–1524.

Rochette, P., Jackson, M. & Aubourg, C. (1992). Rock magnetism and the interpretation of anisotropy of magnetic susceptibility. *Reviews in Geophysics* **30**, 209–226.

Rochette, P., Aubourg, C. & Mireille, P. (1999). Is this magnetic fabric normal? A review and case studies in volcanic formations. *Tectonophysics* **307**, 219–234.

Saunders, A. D., Storey, M., Kent, R. W. & Norry, M. J. (1992). Consequences of plume–lithosphere interactions. In: Storey, B. C., Alabaster, T. & Pankhurst, R. J. (eds) *Magmatism and the Causes of Continental Break-up. Geological Society, London, Special Publications* **68**, 41–60.

Smith, R. M. H. (1990). A review of stratigraphy and sedimentary environments of the Karoo Basin of South Africa. *Journal of African Earth Sciences* **10**, 117–137.

Spera, F. J. & Bohrson, W. A. (2004). Open-system magma chamber evolution: an energy-constrained geochemical model incorporating the effects of concurrent eruption, recharge, variable assimilation, and fractional crystallization. *Journal of Petrology* **45**, 2459–2480.

Sun, S. S. & McDonough, W. F. (1989). Chemical and isotopic systematics of oceanic basalts: implications for mantle composition and processes. In: Saunders, A. D. & Norry, M. J. (eds) *Magmatism in the Ocean Basins. Geological Society, London, Special Publications* **42**, 313–345.

Sweeney, R. J., Duncan, A. R. & Erlank, A. J. (1994). Geochemistry and petrogenesis of central Lebombo basalts of the Karoo igneous province. *Journal of Petrology* **35**, 95–125.

Tatsumi, Y. & Hanyu, T. (2003). Geochemical modelling of dehydration and partial melting of subducitng lithosphere: towards a comprehensive understanding of high-Mg andesite formation in the Setouchi volcanic belt, SW Japan. *Geochemistry, Geophysics, Geosystems* **4**, 2003GC000530.

Tauxe, L., Gee, J. S. & Staudigel, H. (1998). Flow directions in dikes from anisotropy of magnetic susceptibility data: the bootstrap way. *Journal of Geophysical Research* **103**, 17775–17790.

Turner, B. R. (1999). Tectonostratigraphical development of the upper Karoo foreland basin: Orogenic unloading versus thermally-induced Gondwana Rifting. *Journal of African Earth Sciences* **28**, 215–238.

Walker, D. A. & McDougall, I. (1982). ^{40}Ar–^{39}Ar and K–Ar dating of altered glassy volcanic rocks: the Dabi volcanics, P.N.G. *Geochimica et Cosmochimica Acta* **46**, 2181–2190.

Yoder, H. S. & Tilley, C. E. (1962). Origin of basalt magmas: an experimental study of natural and synthetic rock systems. *Journal of Petrology* **3**, 342–532.